



Seventh Framework Program FP7-SPACE-2010-1  
Stimulating the development of downstream GMES services

Grant agreement for: Collaborative Project. Small- or medium scale focused research project

Project acronym: **SIDARUS**

Project title: Sea Ice Downstream services for Arctic and Antarctic Users and Stakeholders

Grant agreement no. 262922

Start date of project: 01.01.11

Duration: 36 months

Project coordinator: Nansen Environmental and Remote Sensing Center, Bergen, Norway

### D8.3: Final report on integration and validation

Due date of deliverable: 31.12.2013

Actual submission date: 22.01.2014

Organization name of lead contractor for this deliverable: NERSC

Project co-funded by the European Commission within the Seventh Framework Programme, Theme 6 SPACE		
Dissemination Level		
PU	Public	x
PP	Restricted to other programme participants (including the Commission)	
RE	Restricted to a group specified by the consortium (including the Commission)	
CO	Confidential, only for members of the consortium (including the Commission)	

---

ISSUE	DATE	CHANGE RECORDS	AUTHOR
0.0	09/12/2013	Template	Mohamed, Torill (NERSC)
1	18/01/2014	Draft	All Partners
1.0	20/01/2014	Compiled	Mohamed, Torill (NERSC)

***SUMMARY***

The overall objective of SIDARUS is to develop and implement a set of sea ice downstream services in the area of Marine Safety, Marine and costal environment, and Climate and seasonal forecasting. The products to be developed are high-resolution sea ice and iceberg products from SAR, sea ice albedo, sea ice thickness, sea ice habitat conservation and ice forecasting.

The aim of this document is to show how the products developed by SIDARUS have been validated.

**SIDARUS CONSORTIUM**

<b>Participant no.</b>	<b>Participant organisation name</b>	<b>Short name</b>	<b>Country</b>
1 (Coordinator)	Nansen Environmental and Remote Sensing Center	NERSC	NO
2	Alfred Wegener Institute for Polar and Marine Research	AWI	DE
3	Collecte Localisation Satellites SA	CLS	FR
4	University of Bremen, Institute of Environmental Physics	UB	DE
5	University of Cambridge, Department of Applied Mathematics and Theoretical Physics	UCAM	UK
6	Norwegian Meteorological Institute, Norwegian Ice Service	Met.no	NO
7	Scientific foundation Nansen International Environmental and Remote Sensing Centre	NIERSC	RU
8	B.I. Stepanov Institute of Physics of the National Academy of Sciences of Belarus	IPNASB	BR

No part of this work may be reproduced or used in any form or by any means (graphic, electronic, or mechanical including photocopying, recording, taping, or information storage and retrieval systems) without the written permission of the copyright owner(s) in accordance with the terms of the SIDARUS Consortium Agreement (EC Grant Agreement 262922).

All rights reserved.

This document may change without notice.

---

**TABLE OF CONTENTS**

1	Introduction.....	8
2	Ice water discrimination (NIERSC).....	9
2.1	Overview.....	10
2.2	Examples.....	10
2.3	Validation methods .....	11
2.4	References.....	15
3	Ice drift and deformation (AWI).....	16
3.1	Overview.....	16
3.2	Examples.....	16
3.3	Validation methods .....	17
4	Sea Ice forecasting in the Barents and the Kara Sea (NIERSC).....	19
4.1	Overview.....	19
4.2	Examples.....	20
4.3	Validation methods .....	21
5	Iceberg detection and forecasting in the Antarctica (CLS).....	22
5.1	Overview of the demonstration in Antarctica.....	22
5.2	Examples of products .....	23
5.3	Validation methods for iceberg SAR-based detections in Barents Sea.....	23
6	Sea Ice thickness from L-band passive microwave data (UB) .....	25
6.1	Overview.....	25
6.2	Examples.....	25
6.3	Validation methods .....	27
7	Validation of sea ice thickness in the Arctic from CryoSat data (UCAM, met.no) .....	28
7.1	Overview.....	28
7.2	Examples.....	28
7.3	Validation methods .....	30

8	Ice Albedo and melt ponds in the Arctic (UB) .....	32
8.1	Overview.....	32
8.2	Examples.....	32
8.3	Validation methods .....	34
9	Animal ARGOS tracking .....	36
9.1	Ivory Gull (UB) .....	36
9.1.1	Overview.....	36
9.1.2	Examples.....	36
9.1.3	Validation methods .....	39

## LIST OF REFERENCES

D5.3 "Report on SAR analysis", WP5, SIDARUS project

D8.3 "Final report on integration and validation", WP8, SIDARUS project

D9.11 "Report on demonstration no. 1 and service utility", WP9, SIDARUS project

***LIST OF ABBREVIATIONS***

ASAR	Advanced Synthetic Aperture Radar
AVISO	Archiving, Validation and Interpretation of Satellite Oceanographic data
CNES	French Space Agency
DUACS	Developing Use of Altimetry for Climate Studies
GIS	Geographic information system
GMES	Global Monitoring for Environment and Security
NASA	National Aeronautics and Space Administration
NOAA	National Oceanic and Atmospheric Administration
NRT	Near Real Time
SAR	Synthetic Aperture Radar
SARAL	Satellite with ARGOS and ALtiKa
SSALTO précise	Segment Sol multimissions d'ALTimétrie, d'Orbitographie et de localisation
SSH	Sea Surface Height
SWH	Sea Wave Height

## 1 Introduction

The overall objective of SIDARUS is to develop and implement a set of sea ice downstream services that will extend the present GMES services with new satellite-derived sea ice products. All the SIDARUS products are to be validated with in situ or with data from other satellites. Some validation activities will be documented in the appropriate deliverables of WP4, WP5, WP6 and WP7. The objective of this document is to describe the methods used to validate the products in the frame of WP8 "Data integration and validation". .....

## 2 Ice water discrimination (NIERSC)

Both open water and sea ice have a wide range of backscatter. The difference in backscatter between them can vary significantly depending on wind speed and sea ice properties. The objective of sea ice classification of SAR images is to identify sea ice types basing on surface roughness and other characteristics of the scene. The most straightforward method to employ SAR data for sea ice analysis is to use backscattering coefficients ( $\sigma^0$ ) for discrimination between multiyear, first-year, some young and new ice types and open water, but this method is hampered by ambiguities in the relation between ice types and  $\sigma^0$  (Johannessen et al., 1997; Abreu, 2000), since different ice types and open water in different conditions can have similar  $\sigma^0$  (Dierking, 2010; Sandven et al., 1999). In particular, discrimination between calm open water and first-year ice, new ice or young ice with frost flowers and multiyear ice, based on SAR data, can be problematic (Fetterer et al., 1994). Including into analysis additional image characteristics like image texture and others improves classification results. Another possibility to overcome the problem of different types of sea surface backscatter similarity is by masking the sea ice area in the SAR images basing on additional (usually passive microwave) data.

Several studies have shown that SAR sea ice classification accuracy is improved by using image texture features (Hara et al., 1994; Bogdanov et al., 2005). Texture depends on the spatial scale of sea ice surface and volume inhomogeneity, as well as on radar spatial resolution. Texture features describe spatial variations of image brightness within a group of neighbour pixels large enough to calculate statistically significant estimates. A given texture feature can be different from one ice type to another and reflect variability in sea ice properties sensed by the SAR. The neural network and Bayesian sea ice classification algorithms with the use of texture characteristics for ENVISAT Wideswath SAR data have been developed and described in (Zakhvatkina et al., 2012). In that study, besides radar intensities, eight textural parameters were selected as most informative parameters using statistical analysis. The algorithms showed good applicability in the Central Arctic.

The main task of the NIERSC research within SIDARUS Project has been developing an operational sea ice classification algorithm for SAR images, including its validation. At first, the neural network (NN)-based algorithm has been developed for ENVISAT SAR images (Zakhvatkina et al., 2012). The outcome of satellite data processing was discrimination between level first-year, deformed first-year, multiyear ice and open water/nilas in the high Arctic during winter conditions.

Since in 2012 ESA announced the end of ENVISAT's mission it has become very important to develop an automatic ice classification method for available SAR images. Over the last year of SIDARUS Project NIERSC has worked on creating and establishing a new automatic sea ice classification algorithm to process RADARSAT-2 data. Neural Network (NN) technique worked with RADARSAT-2 data too, however the results of classification were not always satisfactory. The study has been carried out to find the best procedure for RADARSAT-2 sea ice classification. It was found that Support Vector Machines (SVM) approach, which is a supervised learning method, provides the best results. The learning procedure involved the step of comparing expert classification results with K-means automatic classification in order to find the optimal number of generated classes/ The algorithm is developed for images of HH and HV polarization, for data that has a nominal swath width of 500 km and a pixel spacing of 50 m  $\times$  50 m.

The developed sea ice automatic classification algorithm consists of the following steps:

1. RADARSAT-2 raw data preprocessing. This stage includes backscatter coefficients calculation, angular dependence correction and noise reduction of HV- polarization image.
2. Textural characteristics calculation. The choice of most informative textural parameters has been carried out using statistical analysis. The texture characteristics selected are correlation, inertia, cluster prominence, energy, homogeneity, and entropy, as well as 3rd and 4th central statistical moments of image brightness. Those textural features and backscattering intensities for HH- and HV-polarizations are used as basic data for sea ice/ water classification.
3. Support Vector Machines classification using trained SVM. The result map is composed of several classes, including two classes of ice, two classes of water and the land. To incorporate the effect of wind in the classification procedure, it distinguishes between calm and rough water surfaces.

The details of the mentioned steps of RADARSAT-2 SAR data processing can be found in the Report D5.5.

## 2.1 Overview

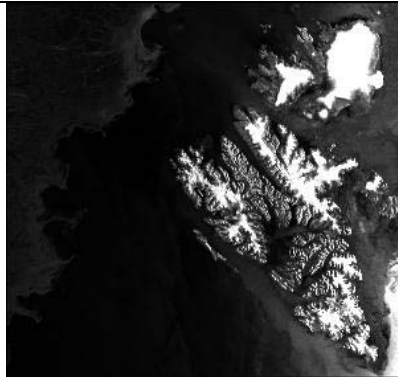
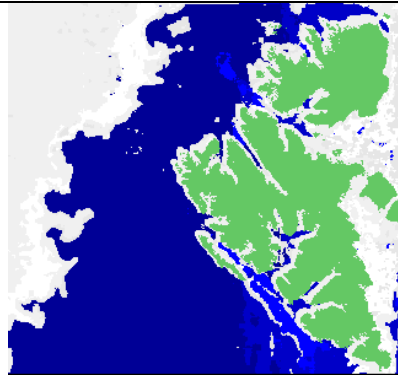
The products generated by the algorithm are sea ice charts showing areas of open water, sea ice and land in the area between Greenland, Franz Joseph Land and Novaya Zemlya. The ice charts are produced through the analyses of RADARSAT-2 ScanSAR Wide Beam mode images. The algorithm is developed for images of HH and HV polarization, for data that has a nominal swath width of 500 km and a pixel spacing of 50 m × 50 m. The product can capture attention of people and services when it is important to know the position of the ice edge with minimum time delay.

The described above algorithm makes the base of the on-line service of sea ice classification available at <http://web.nersc.no/project/maires/catalog.php>. The developed algorithm is an operational one, which means that the ice charts are produced as often as RADARSAT-2 SAR images are received.

## 2.2 Examples

Below there are three examples of sea ice charts for 1-3 January 2014.

In the sea ice charts the ice is shown in white and light grey color, the water is shown in dark and light blue color and the land is shown in green.

Radarsat-2 HH image	Position on the map and date	Sea ice chart (on-line sea ice classification)
	 <p data-bbox="614 1803 710 1870">Гренландское море</p> <p data-bbox="726 1960 869 1993">01.01.2014</p>	

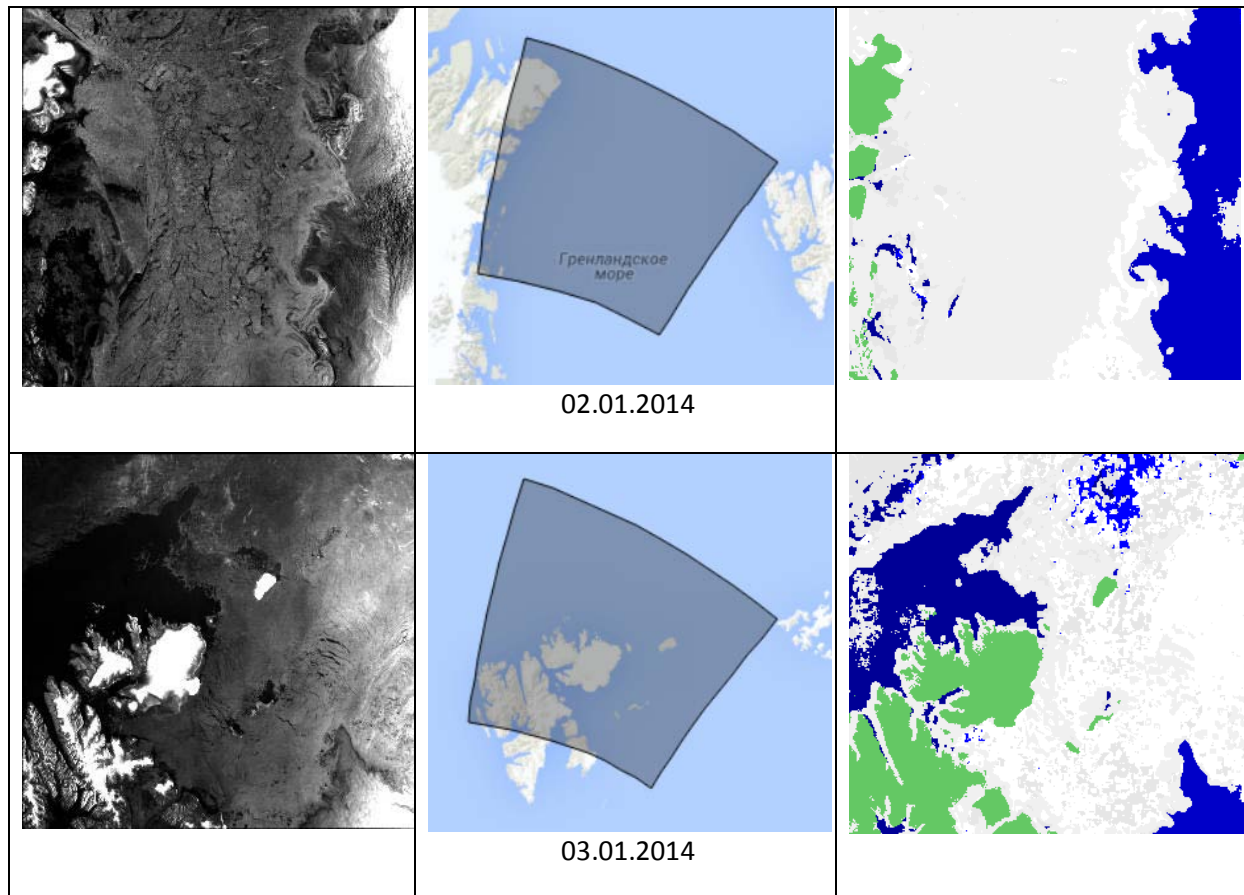


Fig. 2.1. Examples of on-line sea ice classification results.

### 2.3 Validation methods

Sea ice classification results calculated using SVM technique have been compared with Met.no (Norwegian Meteorological Institute) ice charts from the operational ice charting service. Validation of Arctic ice products is always a challenging task due to lack of ground truth data. As a substitute, our product has been intercompared with a manual sea ice product produced by Met.no.

Met.no ice charts are produced by ice analysts at the Norwegian Sea Ice Service using the following data sources: high resolution microwave Synthetic Aperture Radar data (Radarsat), low resolution microwave SSM/I and SSMIS data (DMSP), MODIS data (Terra and Aqua) and AVHRR data from NOAA.

The procedure of Met.no and SVM classification comparison is illustrated by Fig. 2.2. Met.no sea ice type data has been reclassified into charts with only three classes: *open water* (OW), where sea ice concentration values on the original ice map were in the range from 0 to 15% , *sea ice*, where sea ice concentration values were in the range from 15% to 100% and *land*. Our results of SVM classification have been reclassified likewise - into three classes - OW, ice and land. In the comparison Met.no ice charts have been assumed to represent correct classification and we calculated the confusion matrix

(error matrix) keeping in mind that assumption.

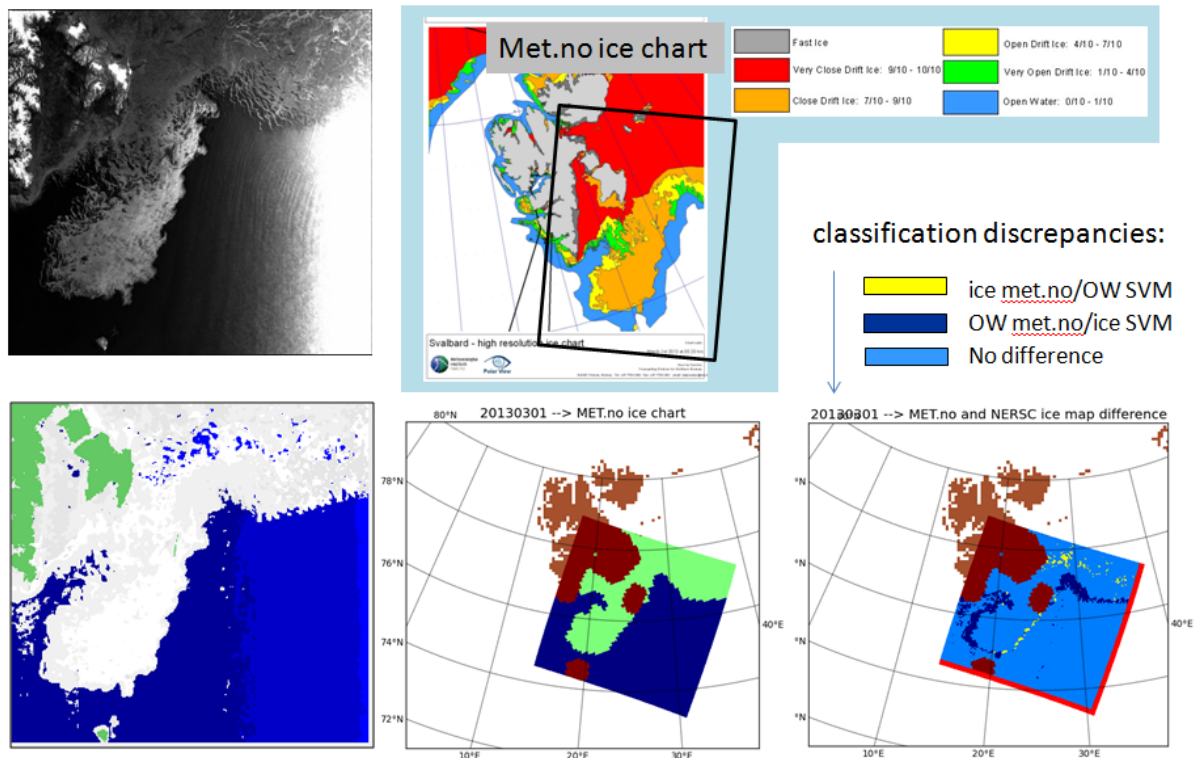


Fig. 2.2. Intercomparison of METNO and SVM ice charts for 01 March 2013.

The overall accuracies of SVM classification were estimated for about 776 Radarsat-2 SAR images received in the period from March – November 2013. The average values of total accuracies for each month are presented in the table below. The accuracy is the ratio of the number of similarly classified pixels on both (Met.no and SVM) ice maps to the whole number of ice and water pixels in the image. The error is the ratio of the number of incorrectly classified pixels of each class to the total number of pixels of that class.

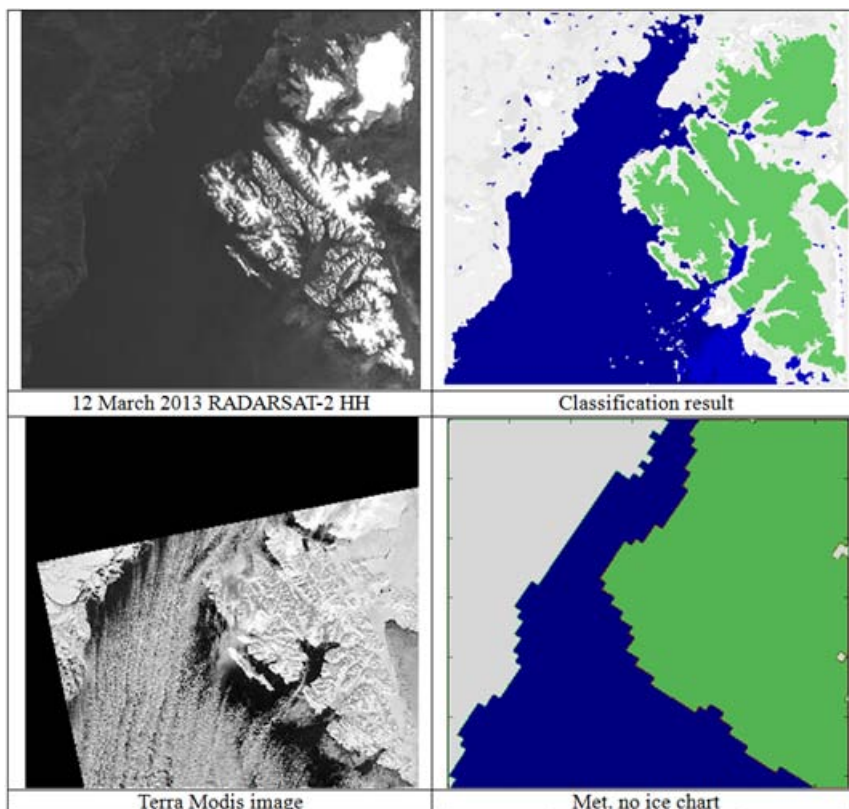
month	Overall accuracy	OW_error	Ice_error
mar	0.92	0.06	0.02
apr	0.92	0.06	0.02
may	0.89	0.08	0.04
jun	0.87	0.11	0.02
jul	0.81	0.16	0.02
aug	0.86	0.12	0.01
sep	0.88	0.11	0.01
oct	0.94	0.05	0.01
nov	0.92	0.07	0.01

The average accuracy of our sea ice classification for the period March-November 2013 is 0.89, being higher in winter (0.92) and lower in summer (0.86). The accuracy is lower in summer months because the SVM classification algorithm was tuned using winter data.

Below several examples of comparison of automated SAR classification and Met.no ice charts are presented. The images are shown in groups. Every group consists of two satellite images and two ice charts: Radarsat-2 HH image and Terra Modis image represent the ice conditions in the scene from the microwave and visual point of view, and two ice charts - the result of our SVM classification and the Met.no sea ice chart - demonstrate how ice conditions are described by automated classification and sea ice analysts. Additionally the confusion matrix is given for every particular pair of ice charts (SVM's result vs. Met.no). In the matrix the correctness of classification for different classes based on pixel-by-pixel differences is shown. The structure of the accuracy/error matrix is the following:

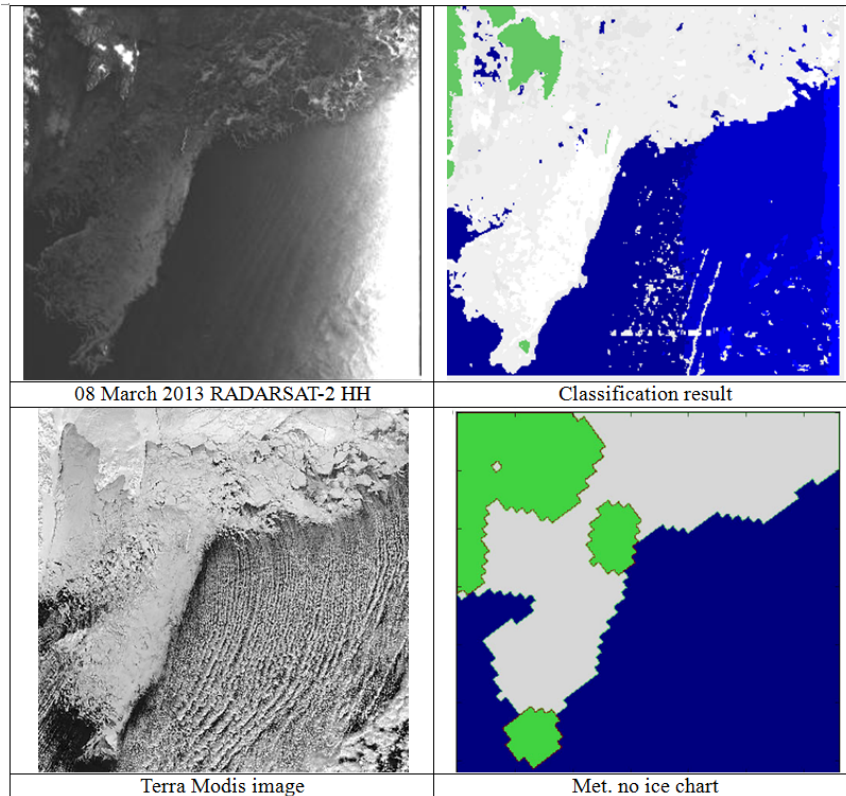
SVM ice classes METNO ice classes	OW	Sea Ice	Unclassified
OW	OW accuracy	SVM sea ice class where there in OW in METNO	Unclassified pixels where there in OW in METNO
Sea Ice	SVM OW class where there is sea ice in METNO	Sea Ice accuracy	Unclassified pixels where there in sea ice in METNO

In the charts below the ice is shown in grey color, water in blue and land in green. Unfortunately only low resolution Met.no ice chart were available for validation.



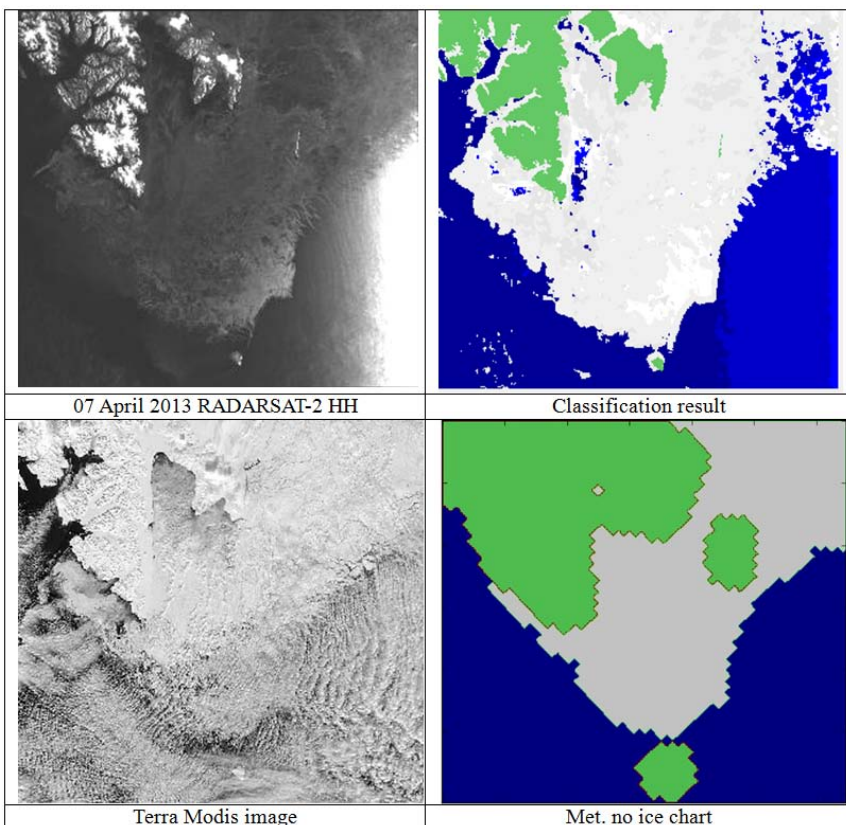
	OW	Sea ice	Un class
OW	96.07	1.67	2.26
Sea ice	6.20	92.83	0.97

overall\_accuracy = 94.24, in percents



	OW	Sea ice	Un class
OW	86.48	12.34	1.18
Sea ice	1.37	96.50	2.13

overall\_accuracy = 90.55, in percents



	OW	Sea ice	Un class
OW	90.91	3.88	5.21
Sea ice	15.48	83.18	1.34

overall\_accuracy = 86.57, in percents

Fig. 2.3. Illustration of validation process. Three automatically produced ice charts are compared with Met.no ice charts of low resolution. The accuracy/error matrix is presented for every pair of ice charts.

## 2.4 References

1. Abreu R. D., "RADAR Sea Ice Signatures: An Operational Primer," in Proc. Workshop on mapping and archiving of sea ice data – the expanding role of radar, Ottawa, Canada, May 2-4 2000. JCOMM Tech. Rep. № 7, pp. 85-94, 2000.
2. Bogdanov A., S. Sandven, O. M. Johannessen, V. Alexandrov, and L. Bobylev, "Multisensor Approach to Automated Classification of Sea Ice," IEEE Trans. Geosci. Remote Sens., vol. 43, no 7, pp. 1648–1664, Jul. 2005.
3. Dierking W., "Mapping of Different Sea Ice Regimes Using Images From Sentinel-1 and ALOS Synthetic Aperture Radar," IEEE Trans. Geosci. Remote Sens., vol. 48, no. 3, pp. 1045-1058, Mar. 2010.
4. Fetterer, F., Gineris, D. and Kwok, R. (1994). "Sea ice type maps from Alaska Synthetic Aperture Radar Facility imagery: An assessment.," J. Geophys. Res., 99: doi: 10.1029/94JC01911. issn: 0148-0227.
5. Hara Y., R. G. Atkins, R. T. Shin, J. A. Kong, S. H. Yueh, and R. Kwok, "Application of Neural Networks to Radar Image Classification," IEEE Trans. Geosci. Remote Sens., vol. 32, no 1, pp. 100–109, Jan. 1994.
6. Johannessen O. M., A. Volkov, V. Grischenko, L. Bobylev, V. Asmus, T. Hamre, K. Kloster, V. Melentyev, S. Sandven, V. Smirnov, J. Solhaug, and L. Zaitsev, "ICEWACH: Ice SAR monitoring of the Northern Sea Route," in Operational Oceanography: The Challenge for European Cooperation - Proc. of the First Int. Conference on EuroGOOS, 7-10 Oct. 1996, J. H. Stell, H. W. A. Behrens, J. C. Borst, L. J. Droppert, Eds. Elsevier, The Hauge, The Netherlands: Elsevier Oceanography Series № 62, 1997, pp. 224-233.
7. Sandven S. , O. M. Johannessen, M. W. Miles, L. H. Pettersson and K. Kloster, "Barents Sea Seasonal Ice Zone Features and Processes from ERS-1 Synthetic Aperture Radar: Seasonal Ice Zone Experiment 1992," J. Geophys. Res., vol. 104, no C7, pp. 15843–15857, 1999.
8. Zakhvatkina N., V. Alexandrov, O.M. Johannessen, S. Sandven, I. Frolov. Classification of sea ice types in ENVISAT synthetic aperture radar images. IEEE Transactions on Geoscience and Remote Sensing, 10.1109/TGRS. 2012. 2212445. vol.51, issue 5, pp. 2587-2600.

### 3 Ice drift and deformation (AWI)

#### 3.1 Overview

Information on sea ice drift and deformation is important both for maritime operations and for polar research. On ships and offshore platforms, maps of ice drift can be used to provide information on the ice movement relative to the ship's track or a forecast of expected ice conditions for the next few days (also considering the wind). Deformation maps show where the ice motion is convergent or divergent. In the former case, one can expect that deformation structures such as ridges or rubble fields come into being, in the latter case leads may be created. Such information is essential for ship route planning or for assessing potential hazards for stationary offshore platforms. In polar research, such information is used to study air-ice-ocean interaction and to improve or validate models for simulating sea ice dynamics. Sea ice drift data can be automatically retrieved from pairs of satellite data. Usually, one uses imaging radar for this purpose since it is independent of light conditions and cloud coverage. Drift products are generated from a pair of two images, hence drift velocity and direction represent the effective displacement of the ice, normalized by the time interval between the acquisitions of the two images. The spatial resolution of the retrieved drift field depends on the SAR image mode used. From image products with high resolution (but narrow coverage of only a few tens of kilometers), one obtains very detailed local drift information on the order of a few tens of meters. If a larger area needs to be covered, Widescan or ScanSAR images are used which provide the drift field for regions of 100-400 km width but with a spatial resolution of a few kilometers.

#### 3.2 Examples

Maps of sea ice drift are usually showing arrows with their lengths being a measure for the velocity, and their orientation reveals drift direction (see Figure 3.1).

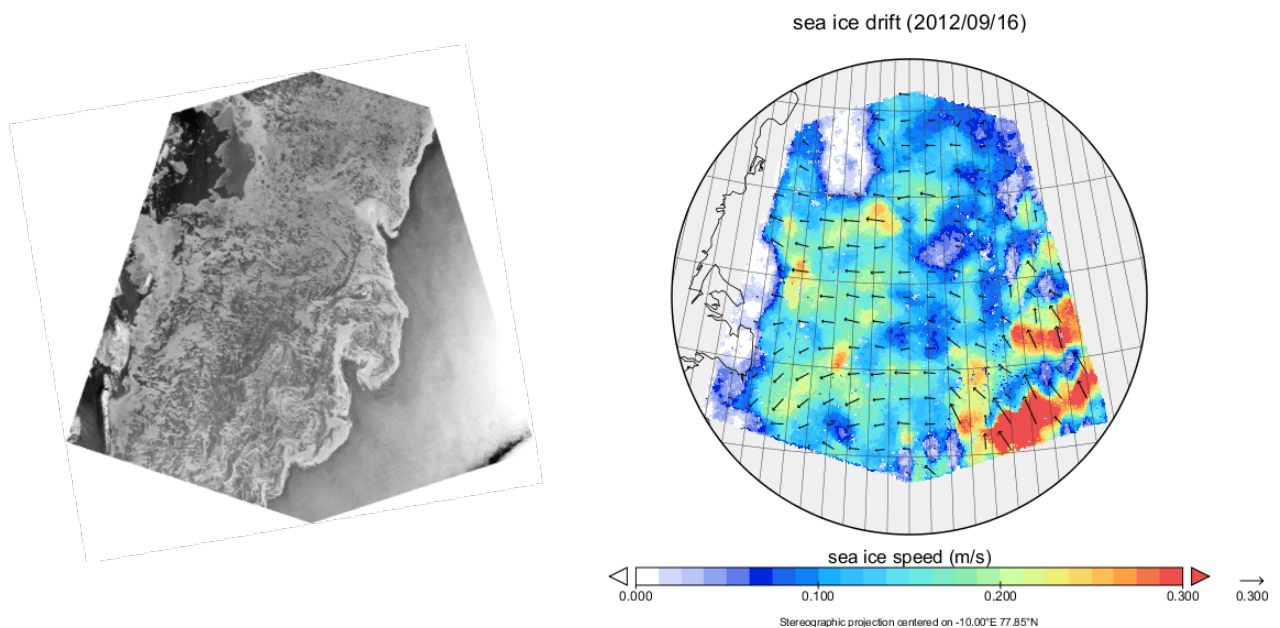


Figure 3.1. Left: Radarsat-2 ScanSAR product from Fram Strait showing the ice condition in the first scene of the image pair used to calculate the ice drift. Right: Resulting drift field.

The resulting drift vectors are valid for the window that was used for phase and cross-correlation analysis in the final step of the retrieval algorithm. Hence, the arrows are given on a discrete grid. Dependent on the size of the figure, the grid may be coarsened and not every arrow may be shown. The discrete velocity values can be interpolated and the result be represented by a color scheme underlying the arrows as in the example of Fig. 3.1. Note that the open water area in Fig. 3.1 was not masked in the analysis, resulting in velocity vectors over open water.

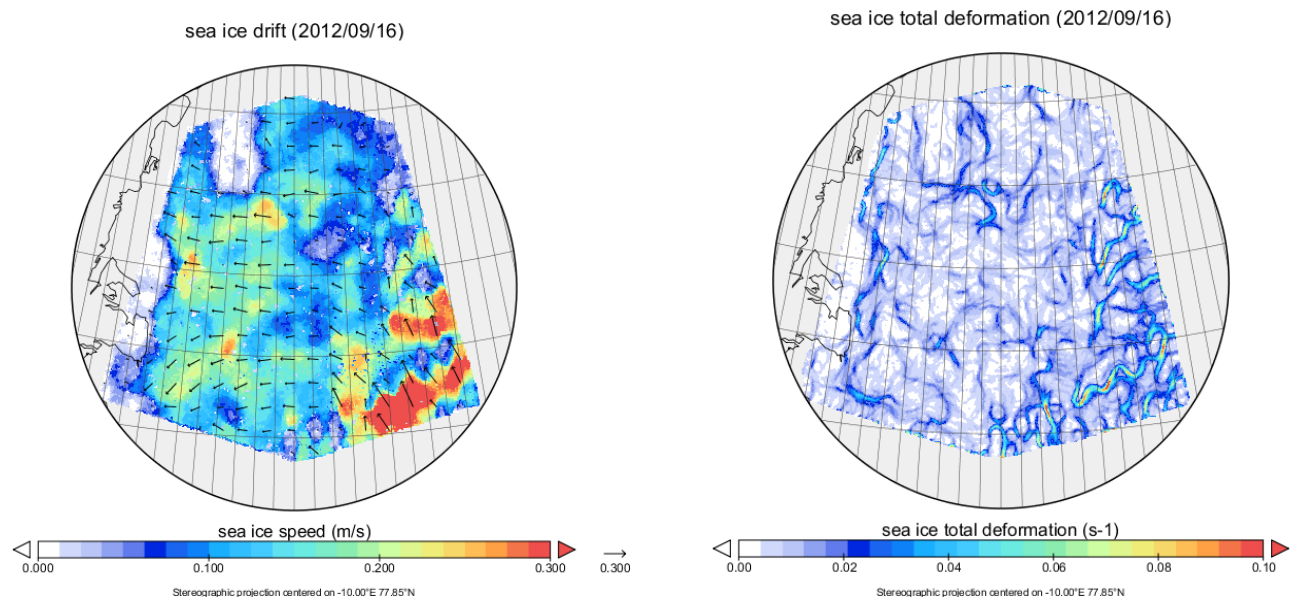


Figure 3.2. Right: Total sea ice deformation. Left: Velocity field from Fig. 3.1 for comparison.

Sea ice deformation can be characterized by different parameters, e. g. total deformation (shown in Fig. 3.2), convergence/divergence and vorticity (the latter as indication for rotational motion components). The intensity of deformation is represented as a color code.

### 3.3 Validation methods

The validation of ice drift fields retrieved from satellite imagery can be carried out using drifting buoys. However, the number of buoys deployed in Arctic or Antarctic waters is small, and in a lot of scenes, a buoy may not be present at all. But even if this is the case, only a very limited area in the satellite-derived drift map is covered by the buoy track. Another well-suited possibility is the manual generation of a reference drift field by an experienced operator, which is then used for comparison with the automatically retrieved result. This procedure can only be carried out for a few examples but not for every image pair used in operational mapping. In the framework of the SIDARUS project, a proxy for the accuracy was developed that provides information whether the retrieved drift vectors are reliable. A robust method is to carry out the drift calculations two times, the second time using image 2 as starting point (back-matching). This approach, however, doubles the computation time. Therefore, another measure is introduced in addition that combines the analysis of textural and correlation parameters in a confidence factor (CFA). The CFA takes into account six parameters. Three of them are from the field of image texture analysis, namely the mean intensity gradient (MIG), the mean gradient slope (MGS), and the variance-to-squared-mean ratio (VMR). The fourth is simply

an intensity threshold that reduces the effect of mirror reflections from the ice. These four parameters characterize the properties of each individual image but do not reflect any links between a pair of images. Therefore the correlation coefficient and its confidence interval are included in the reliability assessment. A result of such a reliability assessment is shown in Fig. 3.3. Sea ice deformation parameters are calculated using the drift field as input, hence their accuracy depends on the accuracy of the drift vectors. Also the ratio between spatial extension of the deformation structure and the grid used to calculate the drift, as well as the spatial resolution of the SAR images, have an influence on the uncertainties in the deformation parameters. Quantitative studies of the accuracy of different deformation parameters were not planned for SIDARUS but are recently carried out as a follow-on investigation.

sea ice drift reliability from backmatching (2012/09/16)

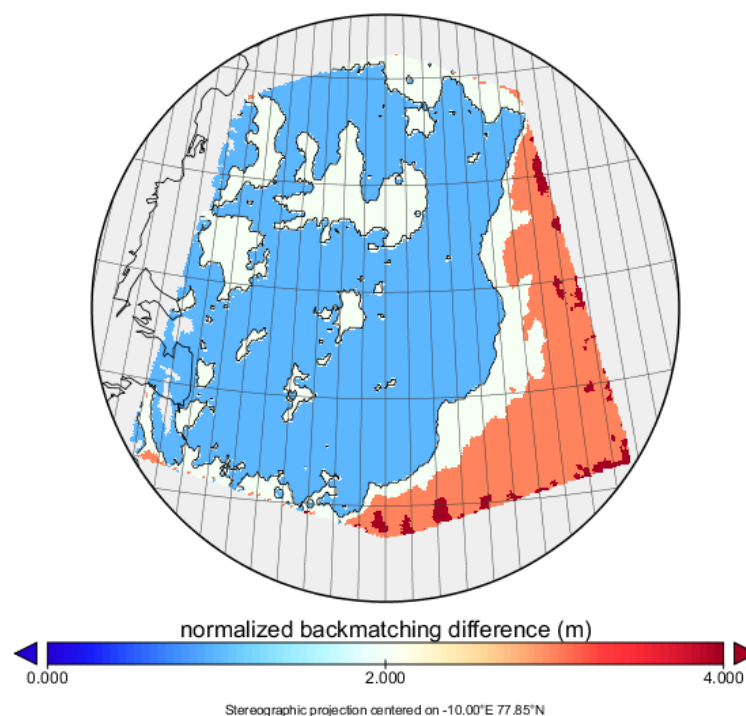


Figure 3.3. Reliability indicator from the Radarsat-2 image shown in Fig. 3.1. Red and white areas are characterized by large back-matching differences, while blue regions are considered reliable.

## 4 Sea Ice forecasting in the Barents and the Kara Sea (NERSC)

### 4.1 Overview

Offshore activities in the Barents and Kara Seas have increased during the last years following new oil and gas exploration in the area. Fishery in Barents Sea is economically important both for Norway and Russia and increased offshore activities may have impact on the ecologically sensitive system in the area. Increased offshore activities and related transportation lead to a demand for a higher preparation for oil-spill recovery operations. For any kind of operations in the Barents and Kara Seas, good forecasts of weather, ocean, wave, and sea ice conditions are essential. The present work focus on the capability to model and forecast the sea ice conditions with focus on the development of the marginal ice zone (MIZ) model.

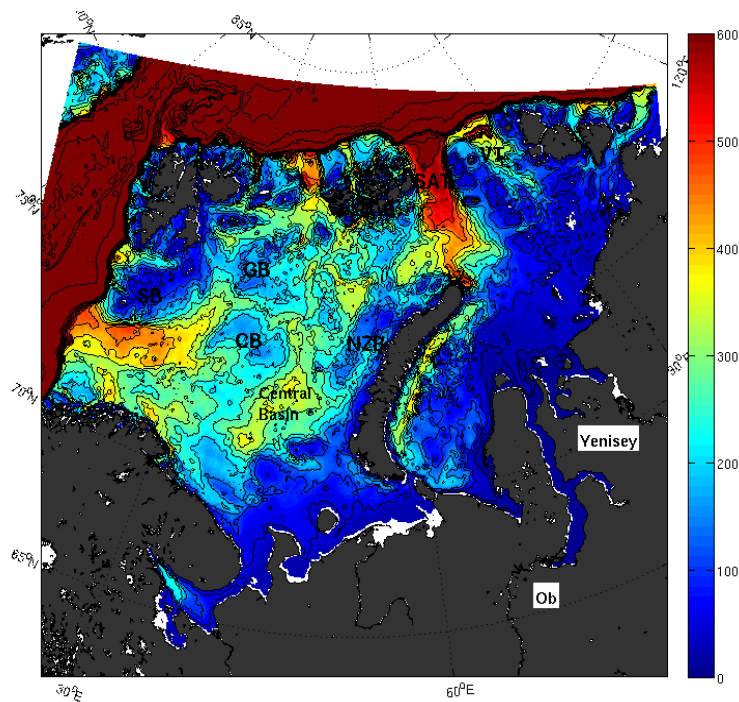


Figure 4.1 Bathymetry used in the Barents and Kara Sea model, with the larges rivers, Ob and Yenisey, indicated as well as the Central Basin, Central Bank (CB), Great Bank (GB), Svalbard Bank (SB), Novaya Zemlya Bank (NZZ), St. Anna Trough (ST), and Veronin Trough (VT). The colour scale is limited down to 600 m depth to highlight the bathymetry on the shelf. Non-coloured areas are outside the model domain and indicate the open boundaries in the north and the west.

The regional model over the Barents and Kara Seas (BS1) covers the area of the Barents Sea and the Kara Sea as well as a some parts of the areas in the Fram Strait, Nordic Seas, and Arctic Ocean, see Figure 4.1. A high-resolution 510x450 grid is applied, that gives approximately a 5 km horizontal resolution. The TOPAZ model and data assimilation system developed at NERSC (TP4) is the main monitoring forecasting system for the Arctic region within the MyOcean project. The forecast for the North Atlantic and the Arctic Ocean (TP4) is used as an outer model in a nested system. Initial conditions are taken from the assimilated TOPAZ system operated by the Norwegian Meteorological Institute (met.no). The regional BS1 model runs on a daily basis producing a 3 days (or 2 days with the wave-in-ice module) forecast of sea ice and ocean conditions.

A webpage is constructed and maintained where the daily sea ice forecasts are presented. An automatic system is setup that downloads forcing fields, validation data, run the TP4 and the BS1 model, produce figures, and update the webpage. The webpage also include a Validation section where earlier forecast are compared with OSI-SAF sea ice concentration fields. Earlier forecasts are found in the Archive section. A short System Description and Updates are also included. Today there are two parallel forecasts presented at two webpages, the first only include the EVP + MIZ sea ice rheologies, <http://topaz.nersc.no/Knut/IceForecast/Barents>, and the forecast also including the wave-in-ice module (EVP + MIZ + WIM), <http://topaz.nersc.no/Knut/IceForecast/Barents2>.

## 4.2 Examples

On a daily basis are a forecast presented on the webpage. There are three different products presented for the EVP+MIZ, i) sea ice concentration with sea ice velocity vectors on top, ii) absolute value of sea ice speed, and iii) sea ice thickness, see Figure 4.2 a), b), and c) respectively. For the EVP+MIZ+WIM forecast is also the maximum floe size presented, see Figure 4.2 d), as well as the position of the MIZ shown as a line on top. The MIZ area is defined to the area where the maximum floe size is less than 200 m, see Figure 4.2.

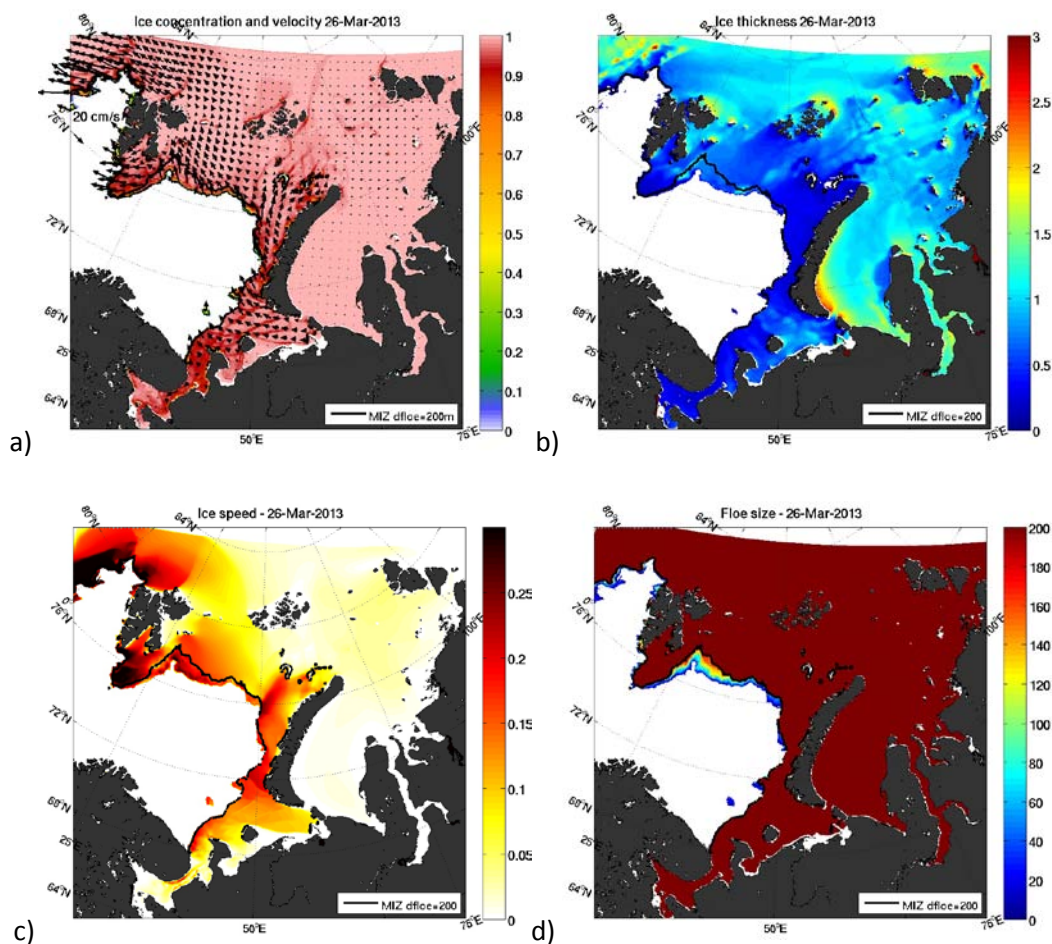


Figure 4. 2. Forecast with the WIM forecast model for the 26th of Mars 2013, a) sea ice concentration and velocity, b) sea ice thickness (m), c) absolute sea ice velocity (m/s), and d) maximum floe size (m) produced by the WIM module. The transition from MIZ to pack ice is indicated by the 200m floe size line (black).

...

### 4.3 Validation methods

On a daily basis a validation is done, where the first day forecast four days ago of sea ice concentration is compared to OSI-SAF sea ice concentrations. The 15% OSI-SAF concentration line is plotted on top of the model sea ice concentration and on top of other forecast products.

Further validation has been done off-line. In general does the forecast model follow the seasonal variability and respond correct to atmospheric forcing, though without direct assimilation within the regional model, some major deviations from measurements are seen. I) The transition from no ice to high sea ice concentration is too sharp in the model compared to OSI-SAF data, see Figure 4.3 a) and b). II) Too much sea ice is seen north of Svalbard and west of Novaya Zemlya during most of the winter season. III) Even in sea ice thickness does the model have a too sharp transition from thin towards thicker sea ice compared to SMOS sea ice thickness, see Figure 4.3 c) and d).

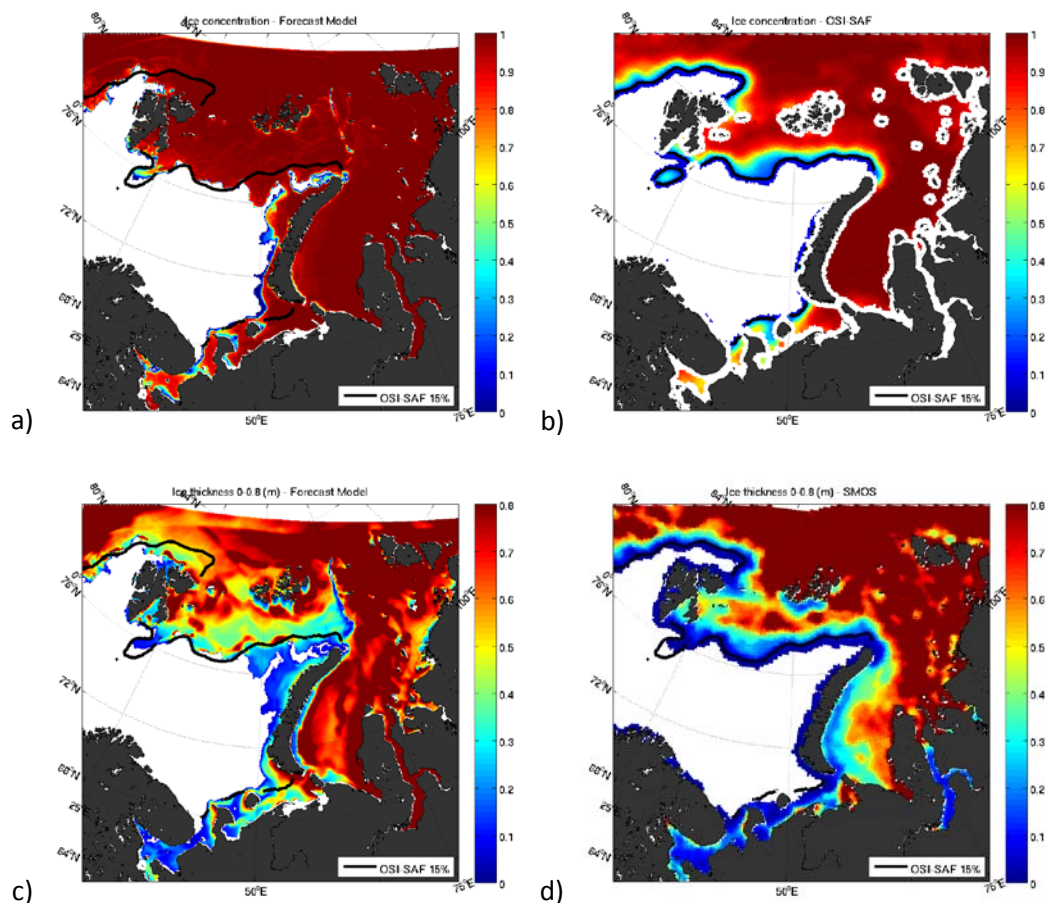


Figure 4.3. Comparing sea ice concentration from a) the model and b) OSI-SAF data and sea ice thickness from c) model and d) SMOSIce thin sea ice thickness.

## 5 Iceberg detection and forecasting in the Antarctica (CLS)

### 5.1 Overview of the demonstration in Antarctica

The Vendée Globe is a round-the-world single-handed yacht race, sailed non-stop and without assistance. The race was founded by Philippe Jeantot in 1989, and since 1992 has taken place every four years. The 2012-2013 edition started on November 10, 2012 with 20 participants. The race is open to monohull yachts conforming to the Open 60 class criteria (overall length, draught, appendages and stability, as well as numerous other safety features).

The service started some days prior the arrival of sailboat in Antarctica and finished when the last sailboat crossed the last dangerous area (i.e the Cape Horn). The demonstration is aimed at the race organization who is then in charge of the dissemination of the delivered products to the sailboats. The race director uses CLS iceberg products to set "ice gates".



Figure 5. 4 Planned route of sailboats for the VG2012, with location of ice gates (from Vendee Globe official website)

As stated by the Vendee Globe (see <http://www.vendeeglobe.org/en/news/article/1396/how-ice-gates-work.html>), "an Ice Gate is a segment on a given latitude, defined between two longitudes. The space between the longitudes is around 400 miles, the equivalent of one and a half day of sailing. There are four to six, or sometimes seven gates along the route and they are spaced out between 800 and 2,000 miles. In order to validate their crossing, skippers only need to sail through the gate from north to south, from south to north, or just keeping sailing north. "

The products are produced in kml format with information of detected icebergs, and their drift in the near future.

## 5.2 Examples of products

On the 26 November, the first ice gate has been moved well in advance the arrival of the first sailboat. As seen by the Figure 5.2, detected icebergs are then drifted with the drift model (represented by the white lines), and the final “averaged” locations are represented by dots with red or orange tiles depending on likelihood. See “D9.1: Demonstration of downstream services” for additional information.

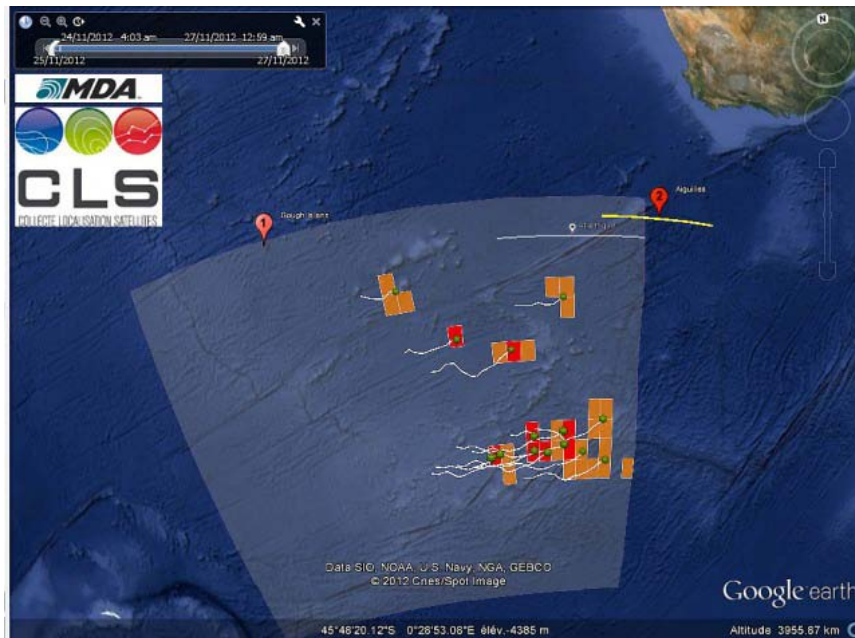


Figure 5.5 Move of the “aiguilles ice gate”

...

## 5.3 Validation methods for iceberg SAR-based detections in Barents Sea

The validation for this integrated service (joint use of altimeter and SAR detections, drift modeling) is documented in separate SIDARUS deliverables:

- D5.1: Review of SAR algorithms and toolboxes - > validation of SAR-based detection from ENVISAT ASAR images
- D7.3: Iceberg drifts in Antarctica - > validation of the drift model
- D8.1: Report on integration and validation -> validation of altimeter-based detection

The aforementioned documents mainly report on validation for icebergs in Antarctica (detection/drift of large icebergs in open water).

In this deliverable, some additional activities regarding iceberg detection in Arctic seas are reported. A set of ARGOS beacons has been deployed on icebergs in Barents Sea (Franz Joseph, Nova Zambla...), then some SAR images (from TSX, CSK, RS2...) in different high resolution modes have been acquired over the same areas. Iceberg detection has been finally carried out as a blind benchmark process.

Figure 5.3 below synthesizes the results and intends to highlight some correlation between several parameters (iceberg size, image resolution) and the level of detection.

First of all, no trend can be outlined regarding the acquisition frequency (X- or C-band) or the sensor (CSK, RS2 or TSX). Two main criteria seem of interest for iceberg detectability, i.e. the size (surface extent and above-sea height) of the iceberg with respect to the sensor pixel spacing, and the incidence angle. It should be noted that the results indicate some trends for human-based iceberg detection in sea ice in the case of high-resolution dataset only. They do not include the variability of iceberg shapes which is obviously of high interest (only a limited set of icebergs have been tracked here).

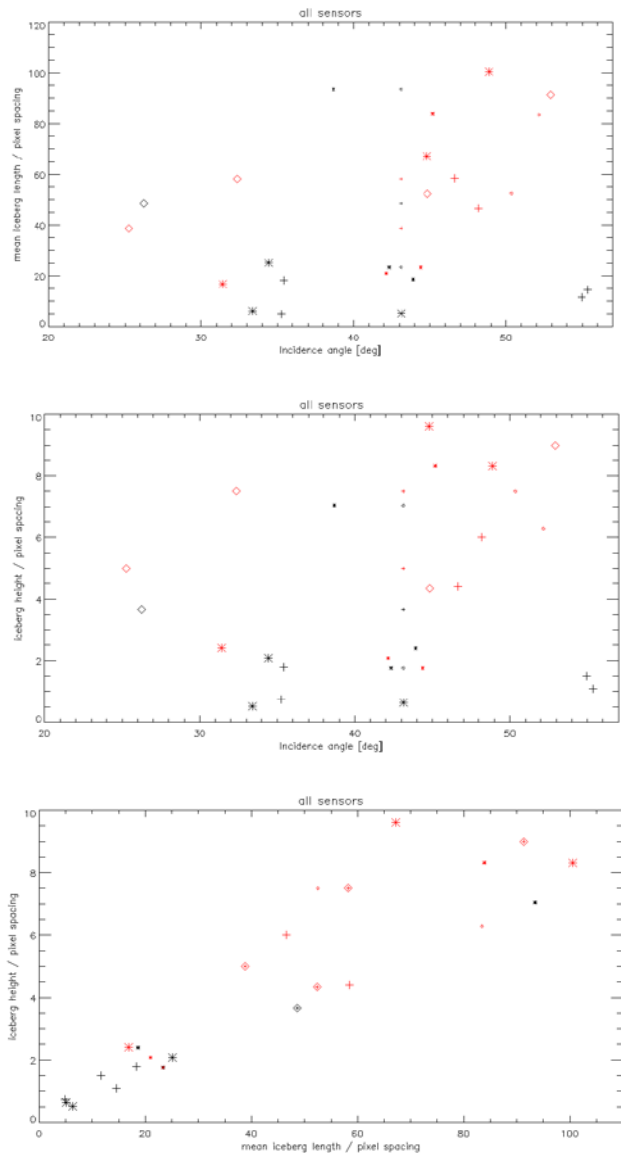


Figure 5.6: Iceberg detectability depending on SAR parameters (sensor, resolution, and incidence angle) and iceberg size (mean length and height) with detected icebergs in red and non detection in black. Sensor: + CSK,  $\diamond$  TSX, \* RS2. Large symbol indicates the cases when there is less than 10 days between SAR acquisition and in situ measurements from ARGOS deployment ©TOTAL/CLS

## 6 Sea Ice thickness from L-band passive microwave data (UB)

### 6.1 Overview

The Soil Moisture and Ocean Salinity (SMOS) satellite carries the Microwave Imaging Radiometer using Aperture Synthesis (MIRAS) instrument recording the full Stokes vector. It works at 1.4GHz (about 20cm wavelength) and covers large areas with multiple overlap in Arctic and Antarctic regions. The sensor geometry allows to observe a single region from different incident angles during one overflight. SMOS data is available in an Icosahedron Snyder Equal Area (ISEA) 4H9 grid with 15km grid spacing. The footprint size varies with incident angle from 30 to 90km, so that data of neighboring grid cells is correlated. Near real time data, where every second grid point is used over ocean, is available and is processed daily with 6 hours delay. The final data is processed daily with 30 hours delay. Passive microwave data at L-band is contaminated by radio frequency interference (RFI) since there are many man-made emissions at this frequency. RFI is filtered in a way that the final product should not be influenced by RFI. However, this filter reduces the Data to 1/3 of its unfiltered volume in the NH. There is nearly no data loss in Antarctica due to RFI.

The acquired brightness temperatures are compared with a cumulative freezing degree day ice growth model in the Kara Sea and Barents Sea in October to December 2010. Empirical functions are fitted for intensity and polarization difference averaged over 40 to 50 degree incident angle, from which a retrieval algorithm is derived. The retrieval algorithm is sensitive to ice thicknesses of freshly frozen sea ice of up to 50cm thickness.

The dataset is in gridded into the polar stereographic National Snow and Ice Data Center (NSIDC) grid with 12.5km grid spacing and is available in GeoTIFF and NetCDF format. A website and processed data from 2010 till present is soon available online at <http://www.iup.uni-bremen.de:8084/SMOS/>.

### 6.2 Examples

As an example for the sea ice thickness retrieval a daily average is shown for the Arctic and Antarctic in Figure 6.1. The beige colored areas indicate ice thicknesses of more than 50cm, open water is shown in blue. The images show the regional early winter, where a slow increase in ice thickness ensures the applicability of the algorithm, which was empirically trained for this conditions. As expected, in Antarctica there is less thin ice than in the Arctic.

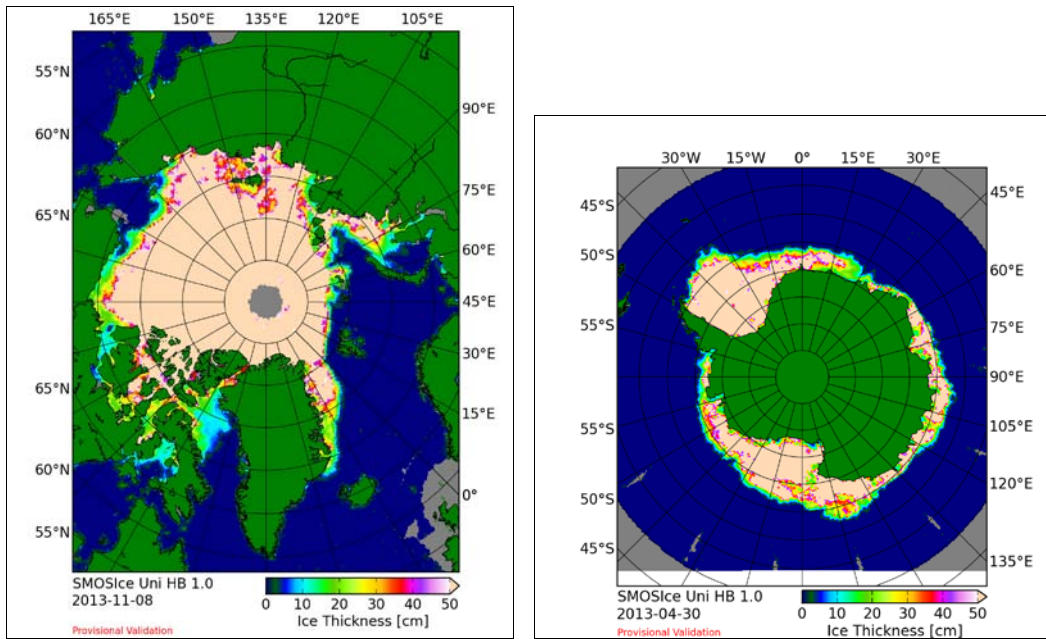


Fig 6.1: Example maps of SMOS sea ice thickness for Arctic and Antarctica showing thin ice regions. Ice thicker than 50cm is colored in beige.

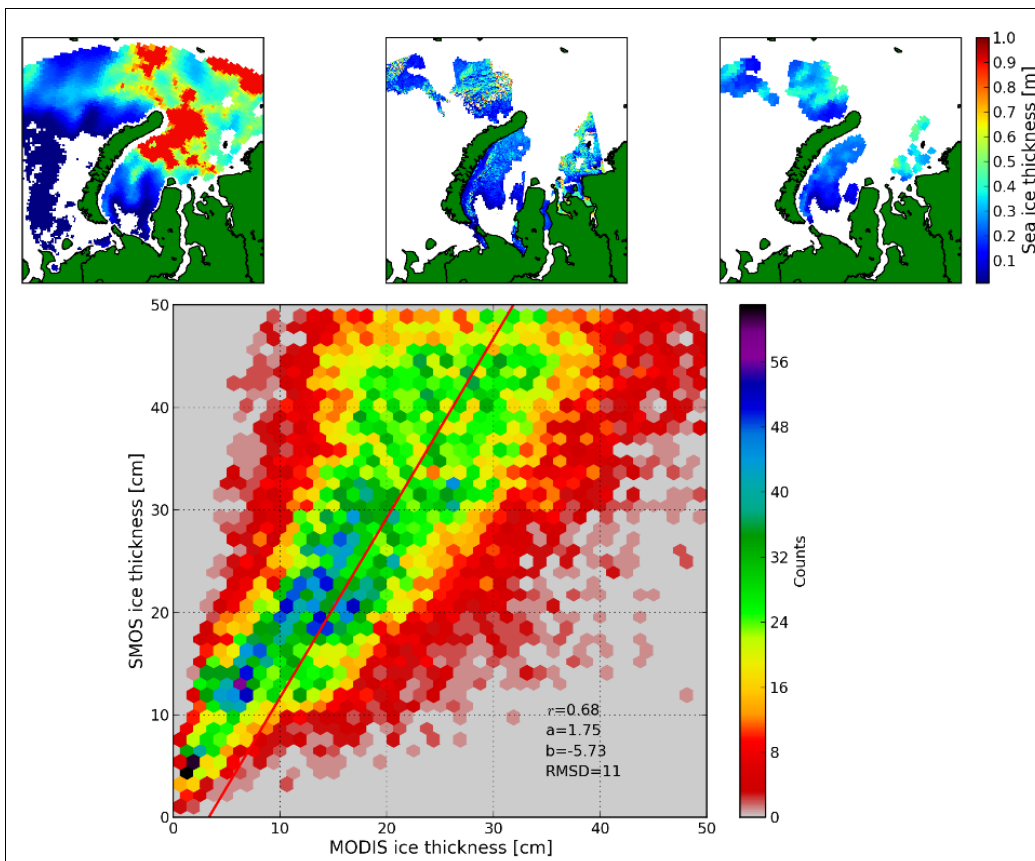


Figure 6.2. Comparison between SMOS (top left) and MODIS (top center) retrieved SIT for 4 Dec. 2010 in the Kara Sea. The valid MODIS data after averaging to the SMOS footprint size (top right). The scatter plot of MODIS and SMOS for all MODIS data from 24 Nov. 2010 to 14. Apr. 2011 (71 scenes) (bottom). Regression line (red):  $y = 1.75x - 5.73$ , RMSD=11 cm, correlation of 0.68.

### 6.3 Validation methods

Validation of thin ice is an important but complicated issue, since it is too thin to stand or walk on it. Therefore the validation of a thin ice thickness retrieval has to rely on other remote sensing data. One source of thin ice data was a night time thermal imagery sea ice thickness retrieval from the Moderate-resolution Imaging Spectroradiometer (MODIS). For Winter 2010/11 71 MODIS scenes are analyzed and compared with the SMOS retrieval showing good agreement especially in lower ice thicknesses as can be seen from Figure 6.2.

Another source of validation Data was the AWI EM-bird instrument which can be carried by a helicopter or airplane which measures every few meters the ice thickness of a footprint of about 50m diameter. Figure 6.3. shows one EM bird flight track and the corresponding SMOS sea ice thickness retrieval. The logarithmic histograms on the left show the distribution of EM bird measured thicknesses with their mean, median, and the SMOS retrieved values at that location number from the right-hand side. Here it is visible that the SMOS retrieval is in nearly all cases exactly at the peak occurrence of EM-bird measured sea ice thickness.

The validation shows that the sea ice thickness retrieval from SMOS works within the indicated limits.

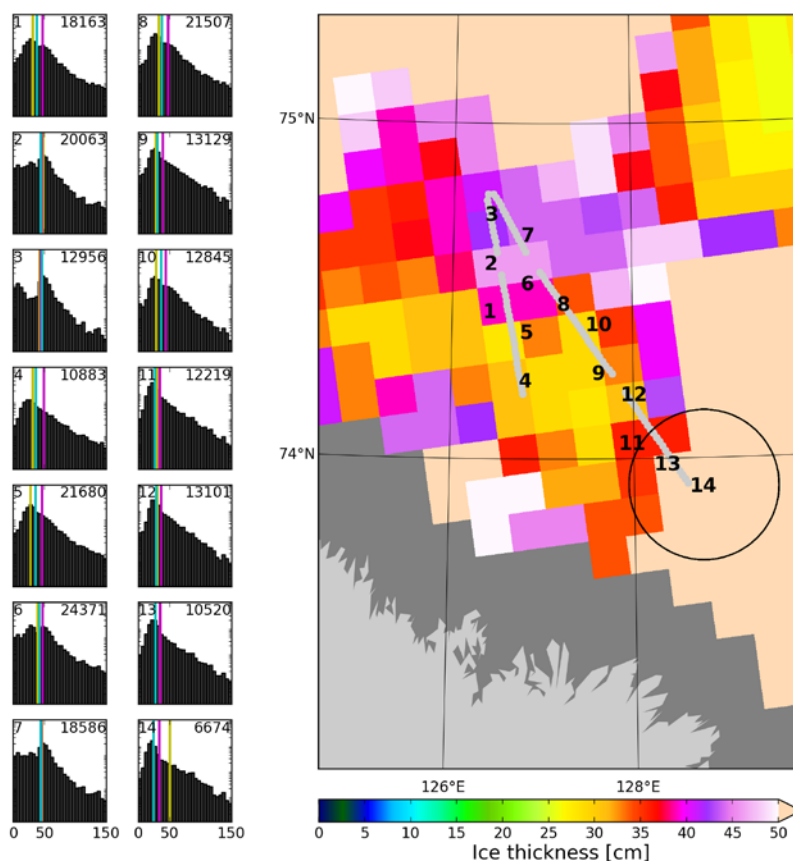


Fig. 6.3. Comparison of EM Bird and SMOS sea ice thicknesses: (right panel) Location of EM bird flight of 20 April, 2012 (grey track) over SMOS retrieved ice thickness (colored background tiles). The large black circle illustrates the average size of a SMOS footprint; (left panel) Histograms of EM bird SIT retrievals within circular regions of SMOS footprint size centered around the same number (upper left of each histogram) on the right-hand image. The number of EM bird measurements for each histogram is shown on the upper right. The colored vertical lines correspond to the mean (purple) and median (cyan) of the EM bird measurements while yellow lines indicate the retrieved sea ice thickness by SMOS.

## 7 Validation of sea ice thickness in the Arctic from CryoSat data (UCAM, met.no)

### 7.1 Overview

The main objective for WP6 was to improve the Cryosat-2 sea ice thickness algorithm with support from in situ and meteorological station data, and ice analyst charts. This task was led by the University of Cambridge (UCAM) in conjunction with the Norwegian Meteorological Institute (Met.no). UCAM led the field campaigns and collected data for sea ice draft (SID) from a submarine-mounted upward-looking sonar (ULS) operating in the Beaufort Sea and Met.no provided support with Radarsat-2 SAR data and ice charts for use in Cryosat-2 comparisons.

The aim of these comparisons were to evaluate the CryoSat-2 capability of distinguishing region and season specific sea ice thicknesses, and allow error bars to be determined for derived average thicknesses. Subsequently positive results from the improved algorithm would lead to implementing Cryosat-2 data into the operational processing chain to automate sea ice thickness measurements. By automating sea ice thickness products the potential errors can be lessened when manually processing data. This benefits core users of the sea ice operational charts for safety in navigation, as well as the science community because they can use these archived automated products as sea ice proxies for future satellite data validations.

CryoSat-2 is a radar altimetry mission that was launched April 2010 to observe ice sheet and sea ice conditions, specifically aimed at observing trends in Arctic sea ice extent. CryoSat-2 operates in the Ku-band (13.575 GHz) and measures Earth's surface from an altitude of approximately 720 km for latitudes up to 88° for the north and south. The main altimeter is called SIRAL (SAR/Interferometric Radar Altimeter) which can operate in three different measurement modes; Low-Resolution Mode (LRM) for ice sheet interiors, SAR for sea ice floes, and Interferometric mode to observe ice sheet margins over mountain glaciers at an inclination of 92°. In CryoSat-2 pulse limited mode, a burst of radar pulses are sent at intervals of approximately 50  $\mu$ s (20000 Hz) and the echo returns are correlated for a swath of 250m wide, 15km long, and a period of 99.2 minutes. The satellite moves forward at 250m for each interval.

Though the use of level 2 CryoSat-2 data was preferred for this comparison due to the inclusion of multiple parameters (i.e. retracker, sea surface height, freeboard, elevation..etc.), a thorough investigation into the development schemes of level 2 data components found no clear literature as to how these were being produced. Since it is difficult to obtain an accurate mean sea surface, the isostatic balance of the ice floe in the ocean makes it difficult to measure sea ice freeboard. Freeboard is the area of ice above the water line. Uncertainties from ice freeboard and density are a primary source of errors when calculating sea ice thickness (Alexandrov, V. et al 2010). Therefore, we extracted the average waveforms from the level 1 data to determine if a criteria can be established in which radar altimetry measurements can detect sea ice thickness variations based on measurements from the waveform amplitudes.

### 7.2 Examples

This two-part effort included data from field campaigns collected by UCAM, as well as remotely

sensed SAR data provided by Met.no and customized sea ice charts. The first part will describe contributions by UCAM, followed by results from Met.no.

Data from upward looking sonar (ULS) have been used for mapping ice bottom topography and SID distribution, but still not all ULS data are processed and error corrected (Wadhams et al., 2011). There are a number of environmental, random and systematic factors, contributing to the accuracy of the sea ice draft, derived from submarine ULS, where the open water and the impact of beamwidth are the most important errors (Rothrock and Wensnahan, 2007). Considering the recent climate change and the high sensitivity of sea ice to climate variability, accurate SID data are required for initiation and validation of climate models and satellite observations. For this purpose and to provide long term accurate data sets of climate variables, the retrieved SID in 2007 from ULS operating on submarine in Beaufort Sea has been error corrected. UCAM used retrieved and error-corrected SID in 2007 from ULS operating on submarine in Beaufort Sea to provide a method for retrieval of SID from ULS with corresponding uncertainty analyses and error correction functions.

The bias correction and open water offset for ULS available sections with 50km spatial resolution are shown in Figure 7.1. and the raw and corrected sea ice draft, derived in March-April 2007 from ULS on submarine in the Beaufort Sea are compared in Figure 7.1.

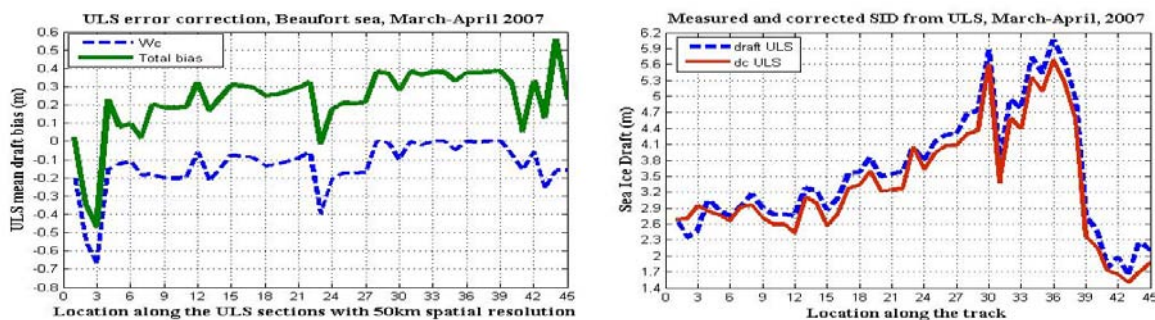


**Figure 7.1.** Water correction offset  $W_c$  and total bias for available data along the track of the submarine (left). Available raw and corrected (red, solid) SID from ULS, 03/2007, along the Submarine track in Beaufort Sea (right).

Only the available data of SID from Beaufort sea in 2007 are biased corrected and can be used for quantitative analyses which are summarised in work package D6.2.

Met.no provided Radarsat-2 Fine Quad-pol mode SAR images obtained from the MyOcean project for the KV *Svalbard* research cruise in April 2011. The Radarsat-2 SAR images were combined with in situ measurements with the aim of extracting relevant data from CryoSat-2 to determine how to improve its capability to detect sea ice thickness. These results were reported in Moen et al, 2013.

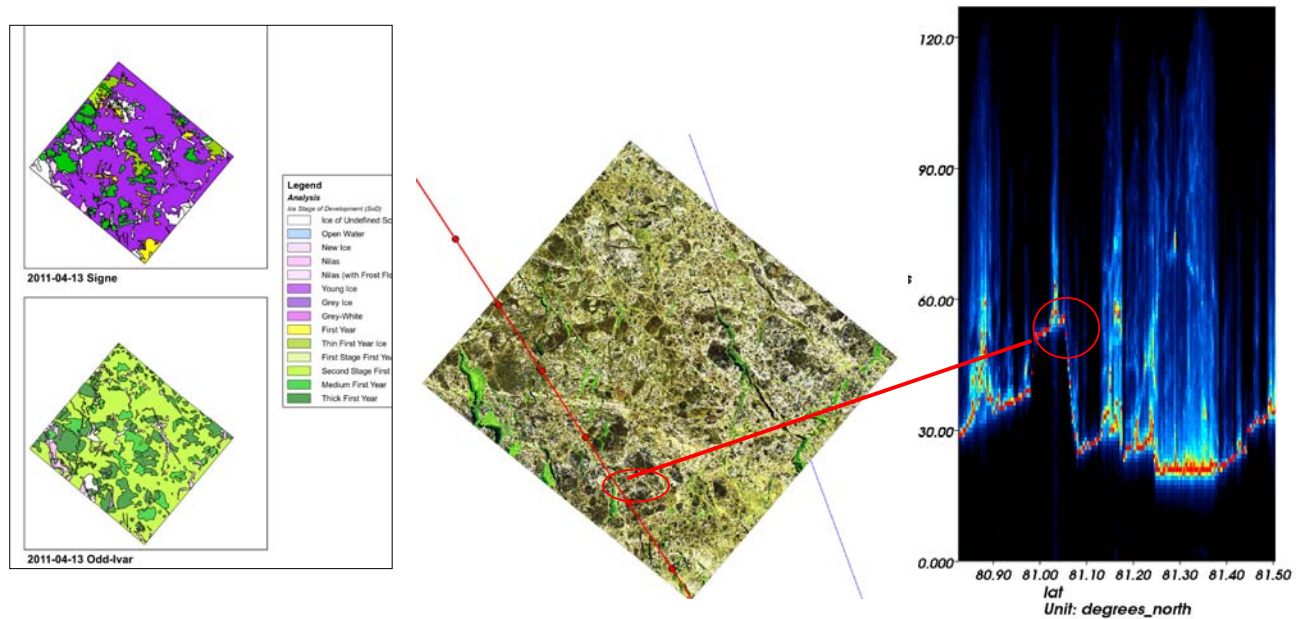


Figure 7.2. Left: Detailed ice charts from the ice service for 11-13, April 2011 corresponding to Radarsat-2 image (middle) and CryoSat-2 level 1b waveform transect (right). The red transect line shows how the waveform could be used to detect thin level ice or leads.

### 7.3 Validation methods

For validation of the CryoSat ice thickness data we have used a set of Radarsat-2 data in Fine Quad-Pole SLC and SGF beam mode. The satellite data have been acquired to coincide with in-situ measurements from two cruises in the Arctic: *KV Svalbard* (6-13 April, 2011) and *Arctic Sunrise* (7-12 July, 2012). Fine quad-pol Radarsat-2 SAR data was used as a ground-truth proxy for sea ice type when compared with CryoSat 2 level 1 waveforms. The CryoSat 2 SIRAL instrument is programmed to operate in SAR mode over sea ice areas, as its measurement footprint has a reduced surface area that allows the detection of smaller sea ice features. Though the use of level 2 CryoSat-2 data was preferred for this comparison due to the inclusion of multiple parameters (i.e. retracker, sea surface height, freeboard, elevation..etc.), investigation of the available products found that these fields had not been calculated. Therefore, we extracted the average waveforms from the level 1 data and converted them to power in Watts with knowledge of the scale factor and power.

Characteristic waveforms over sea ice can theoretically be used to infer sea ice thickness depending on where open water or thin ice areas occur within the waveform (Figure 7.2). However, in order for these waveforms to accurately depict the surface roughness it is necessary to implement the appropriate retracking algorithm. The following retracking algorithms are currently available:

- UCL: ESA retracker
- AWI: Threshold-Spline-Retracker Algorithm
- NOAA: Ocean height based on Maximum Likelihood Estimator
- FMI: Open water and new ice threshold retracker with a Gaussian and
- Traditional OCOG retracker
- Primary peak OCOG retracker

Though several retrackers have been used with previous corrections, specific conditions require different methods of fitting the tracking point on the leading edge and the algorithms vary with each mode. The level 2 data implemented an Offset Centre-of-Gravity (OCOG) and an OCOG threshold retracker but requires further evaluation to resolve errors in the return.

However, in order for these waveforms to accurately depict the surface roughness it is necessary to implement the appropriate retracking algorithm to determine at which point the waveform is actually measuring the surface from a nadir view rather than showing effects of related to noise from how the signal varies in the range direction. Though several retrackers have been used with previous corrections, specific conditions require different methods of fitting the tracking point on the leading edge and the algorithms vary with each mode. The level 2 data implemented an OCOG and an OCOG threshold retracker but requires further evaluation to resolve errors in the return. Therefore, it will be necessary for Met.no to customize thresholds and parameters to the level 1b data to fit the needs of doing a robust comparison with SAR and in situ data.

Demonstrations have been documented in the deliverable D6.2 with a comprehensive description of the Met.no and UCAM contribution.

## 8 Ice Albedo and melt ponds in the Arctic (UB)

### 8.1 Overview

The albedo of the surface and melt pond fraction on sea ice are important parameters which indicate the state of the ice covered Arctic Ocean. These quantities serve as input to GCM and need to be retrieved on global temporal and spatial scales. Within the project, data from MEdium Resolution Imaging Spectrometer (MERIS) sensor were used to perform retrievals of sea ice albedo and melt pond fractions in the Arctic. These two quantities are retrieved simultaneously and are stored in one resulting NetCDF file. The values are gridded into 12.5 km NSIDC grid and averaged over all overflights of one day.

The joint sea ice albedo/melt pond fraction product contains:

- broadband sea ice albedo of the pixel obtained by averaging of retrieved spectral albedos within MERIS wavelength range (400nm-900nm)
- melt pond fraction of the pixel (equals to melt pond fraction of the ice only for ice concentration equal to 100%)
- standard deviation of each grid cell for both sea ice albedo and for melt pond fraction (sources of scatter are: spatial averaging within a grid cell and temporal averaging of several overflights).

Due to solar illumination limitation for a radiometer like MERIS, only summer data are processed (typically, May to September each year.) Spatial data coverage is limited to the ice covered Arctic Ocean (varies with the seasonal cycle). The default output temporal resolution for the user is daily average, processed swath data or weekly averages are available on demand. The daily averages can be downloaded from the UB server under following links:

[http://www.iup.uni-bremen.de:8084/amsredata/meris/June2002\\_2011/](http://www.iup.uni-bremen.de:8084/amsredata/meris/June2002_2011/)

<http://www.iup.uni-bremen.de:8084/amsredata/meris/2009/>

<http://www.iup.uni-bremen.de:8084/amsredata/meris/2010/>

<http://www.iup.uni-bremen.de:8084/amsredata/meris/2011/>

The product is intended for studies of surface properties in the Arctic during melting season, and as input to climate models. For the case when satellite data assimilation into a GCM is impossible, a temporal latitude-dependent parameterization of sea ice albedo has been developed.

### 8.2 Examples

Example of the melt pond fraction product (weekly average is taken to display full coverage of the ice covered Arctic Ocean) is shown in Fig. 8.2.1a for the second week of June 2007. Notice the massive melt in Beaufort sea and relatively melt free MYI areas of the Arctic Ocean. Melt onset starting from south and moving toward the higher latitudes can be seen along the coast of Greenland and at Queen Elisabeth Islands. The developed melt pond fraction and sea ice albedo retrieval algorithm is able to show spatial and temporal dynamics of the pond evolution and sea ice albedo. Fig. 8.2.1b shows the sea ice albedo trend for the third week of June for years 2002-2011. One can see positive albedo trend in the East-Siberian sea, and a negative albedo trend in Beaufort sea and at Queen Elisabeth Islands. Most probably, the reason for the negative albedo trend is not the absolute increase of melt pond fraction or change of ice optical properties, but an earlier melt onset for the region. Whether the same mechanism (i.e. later melt onset) is valid for the East-Siberian sea, it has to be clarified within further studies.

Figure 8.2.2 shows the developed parameterization of broadband sea ice albedo for a set of latitudinal bands, depending on day from melt onset. It was assumed that melt onset starts not earlier than 25 May for latitudes below 76° N, and not earlier than 10 June for higher latitudes. This

parameterization can be used to predict broadband sea ice albedo for a given latitude and date, for the ice covered area of the Arctic Ocean.

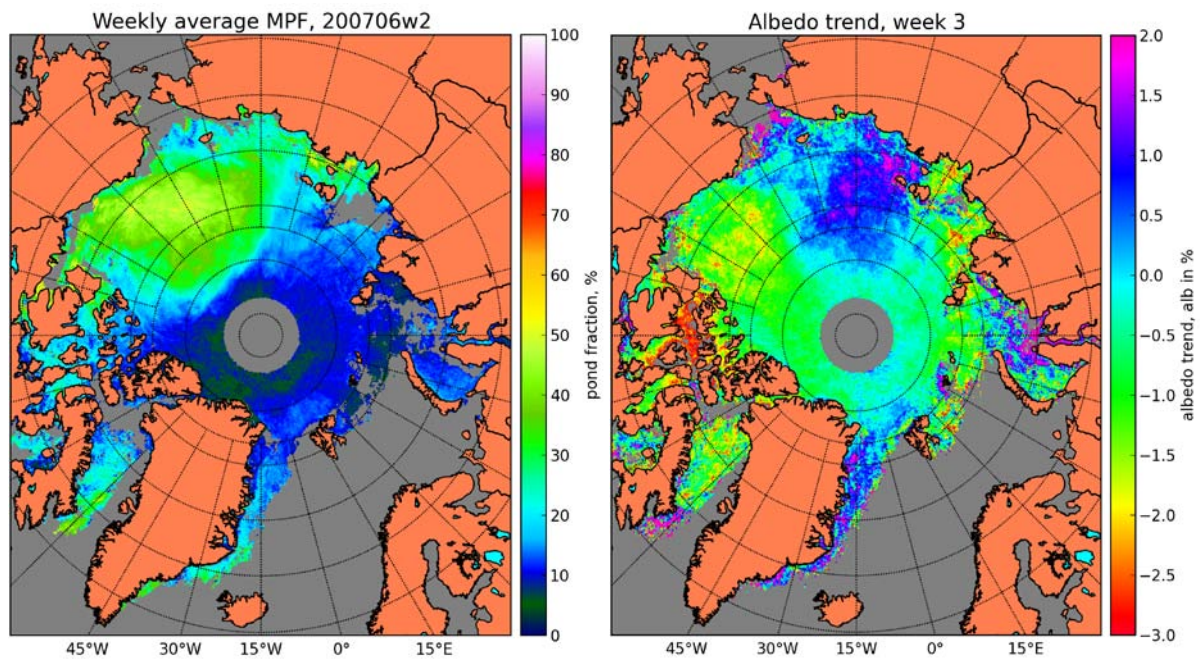


Figure 8.2.1. Example of MERIS products: (a) weekly average of melt pond fraction for the second week of June 2007. Notice the melt onset in Beaufort sea and melt free MYI areas; (b) sea ice albedo trend for the third week of June for years 2002-2011. Notice the positive albedo trend in the East-Siberian Sea and negative albedo trend in the Beaufort sea.

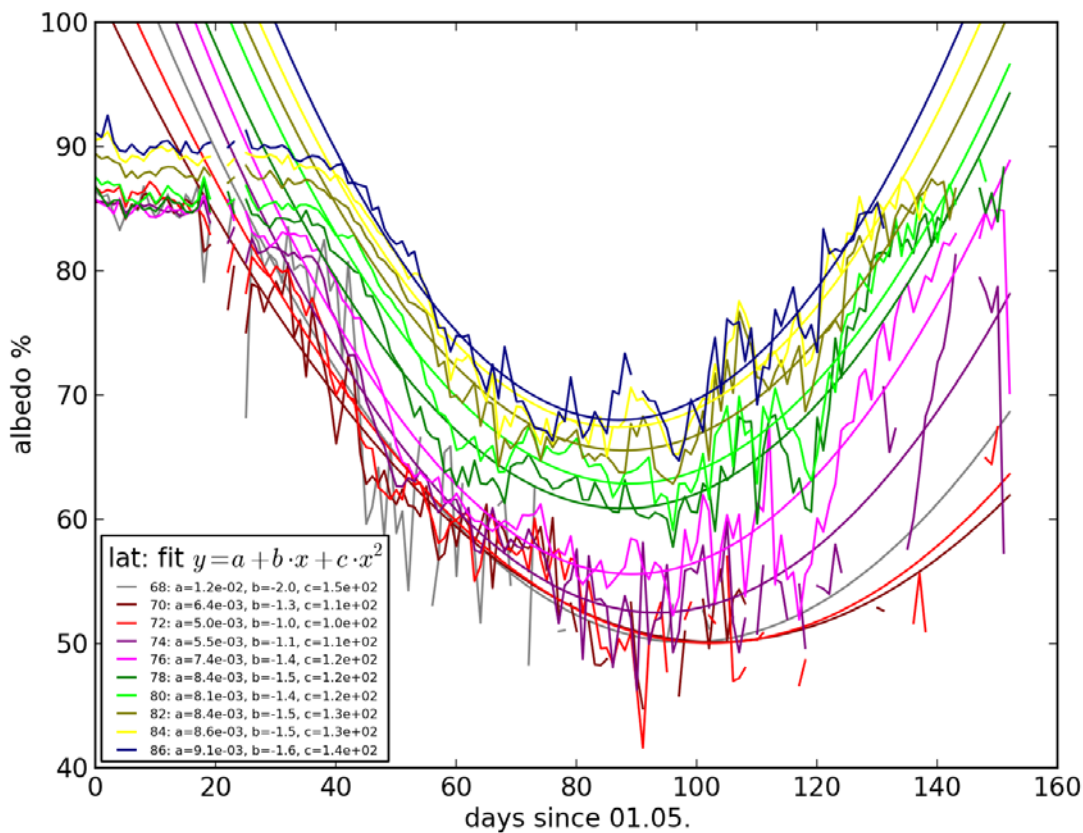


Fig. 8.2.2: Resulting parameterization for the average of the years 2009-2011. The parameterization should not be used before 25 May for latitudes less than 76° N, and before 10 June for higher latitudes.

### 8.3 Validation methods

The MPD algorithm has been validated using a dataset of validation data shown in Table 8.1. The data can be divided into two categories: in situ data (Fig. 8.3.1a) and airborne data (Fig. 8.3.1b). For each category of validation data, a collocation and comparison of retrieved and field value has been performed. The result is shown in Fig. 8.3.1. For the in situ data, the correlation coefficient is 0.526. The observed scatter can be connected to low quality of some validation data (visual estimation of melt pond fraction) and different spatial resolution of the retrieval and the validation data. Here only one example of airborne validation is shown (Fig. 8.3.1b), whereas the whole dataset comprises 10 comparison cases. The correspondence of the MPD retrieved values to the airborne data is reasonably good (40% field value against 50% satellite) with several exceptions which can be explained due to inability of MERIS to resolve the difference between melt pond and so called “blue ice” (sea ice without top scattering layer).

Table 8. 1: Datasets used for validation of the MPD algorithm (authors, location, year, method)

Polashenski, Barrow 2008	In situ field campaign, visual estimation
Polashenski, Barrow 2009	In situ field campaign, fractions along a 200m transect
Birnbaum, MELTEX 2008	Airborne measurements, supervised classification algorithm applied to geolocated quality assured aerial pictures
Birnbaum, NOGRAM 2011	Airborne measurements, supervised classification algorithm applied to geolocated quality assured aerial pictures
Scharien, Canadian Arctic 2002	In situ field campaign, visual estimation
Perovich, HOTRAX 2005	Ship cruise, hourly bridge observations, visual estimation

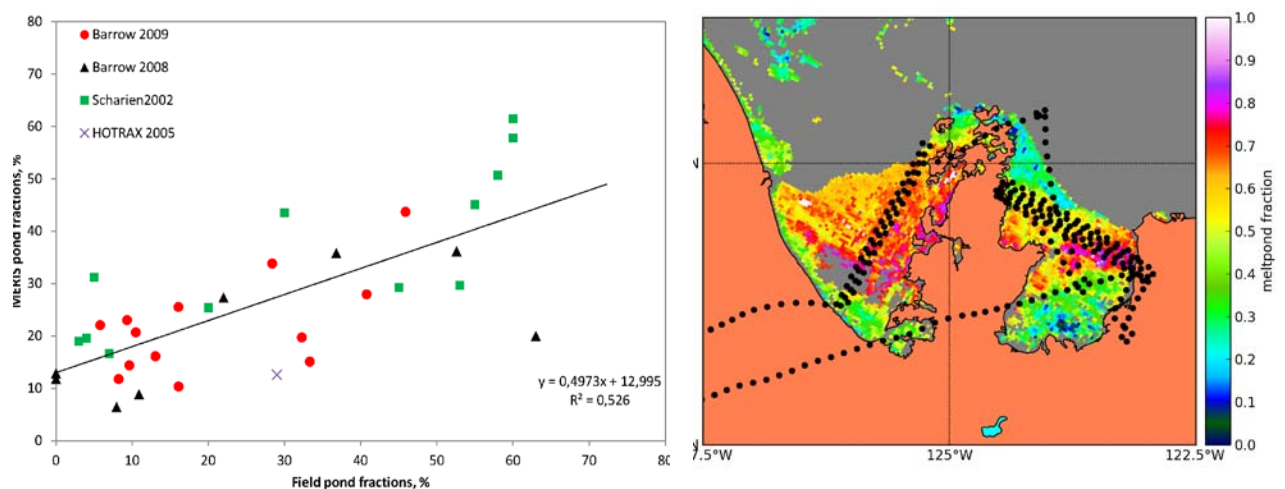


Fig. 8.3.1: Validation of the MPD algorithm against (a) in situ pond fraction measurements, (b) airborne measurements (just one example from MELTEX 2008, 06.06.2008 is shown. Field value: on average 40% melt ponds).

The validation of the MPD retrieval against field data is a challenging task due to lack of validation data which can be collocated with the MERIS data spatially and temporally without being sorted out due to cloud coverage. Another possibility to validate the MPD retrieval is comparison to another remote sensing product. Such comparison attempt has been performed (not shown here) and showed some discrepancies between the MPD retrieval and algorithm by Roesel et al., 2011, from MODIS data. Due to different overflight times of the two sensors (MODIS and MERIS), the cloud coverage and surface coverage might have been slightly different. On the scale of weeks (weekly

averages have been compared), this could have caused some discrepancy. In addition, the difference in accounting for surface reflectance within both retrievals could have been the reason for the disagreement. Further comparison is needed to clarify the issue.

## 9 Animal ARGOS tracking

### 9.1 Ivory Gull (UB)

#### 9.1.1 Overview

The Ivory gull is a threatened species using habitats closely connected to sea ice amount and features. Climate change in the Arctic and especially sea ice decline may affect the migration routes, feeding behavior and breeding areas of this specialist species. Study of ice conditions preferred by the gulls needed to infer the danger to the population caused by the sea ice decline. 42 ivory gulls from Greenland, Arctic Russia and Svalbard have been tagged with ARGOS transmitters and tracked 2007-2011. The objective of this study is to combine gull positions with sea ice concentration data from microwave sensors to retrieve following parameters: Sea ice concentrations at the gull positions and within 10 and 50 km from the gull; histogram of ice concentrations within 50km; distance to ice edge and to the shore. Also, for the defined regions, ice concentration histogram and ice extent of each IC need to be extracted. The resulting dataset is then analyzed for gull preferences of sea ice type, distance to the ice edge, seasonal cycle of preference due to breeding, migration, etc.

The extracted dataset has same temporal resolution as the initial gull position dataset (over 80000 gull positions 2007 – 2011, 42 birds originating from Greenland, Siberia, Svalbard). Its area coverage is defined by the gull location; some of the parameters are delivered on regional to global (whole Arctic Ocean) scales. The dataset is intended for use by biologists and ornithologists studying ivory gull habitat preferences and seasonal behavior. It is produced as a numpy array dataset, but supplied to the user in the format of an Excel sheet. The dataset is available for download on demand by collaboration partners. Its public availability is limited as it includes the original ARGOS position dataset.

#### 9.1.2 Examples

The extraction procedure is organized as a python script employing existing libraries to extract sea ice concentration at a point from dataset at Uni Bremen. The following table describes some of the features of the extracted dataset.

Table 9.1: Columns in the extracted dataset and what they correspond to:

0	index (should be 0, 1, 2, 3 ... since it was sorted before)
1	tag of the gull (should be sorted somehow)
2	Latitude
3	Longitude (lat and lon are the ARGOS position of the gull, not the position of the associated NSIDC grid point.)
4	ic at gull position (directly). It means that just the closest NSIDC grid point is used. This also applies when the gull is at the corner of one grid point so that 3 other grid points can also be very close.
5	ic at gull position (~10km radius average). All grid points with distance to the gull position less than 10km are averaged (for definition of distance see above)
6	ic-std at gull position (~10km radius)
7	ic at gull position (~50km radius average). All grid points with distance to the gull position less than 50km are averaged (for definition of distance, see above)
8	ic-std at gull position (~50km radius)
9	distance to ice edge (in km, approximately +/-3km): The following steps are done for finding the closest ice edge now:

	<p>1) 3 by 3 average spatial is applied to sea ice concentration.</p> <p>2) all areas in this dataset with <math>0 &lt; SIC &lt; 20</math> is determined</p> <p>3) pixels close to land were excluded (<math>&lt; 20\text{km}</math>) since there is possible false sea ice detection.</p> <p>4) monthly climatological masks of sea ice was applied.</p> <p>The distance is positive if the gull is over sea ice or land and negative if over open water. If a gull is close to the coast while there is no ice at that coast, this value will still give the distance to the next sea ice edge i.e. 1 to 20% averaged 3by3 area. On the other hand, if the gull is over sea ice and there is a larger lead, it could have the same properties and the distance to the lead is determined. However, in this case the lead should seem for the gull like open water anyway.</p>
10	distance to coast (in km, approximately +/-3km): gull distance to coast is determined as the closest pixel to the gull distance to the coast, where the coast distance is evaluated for every NSIDC grid point from a 0.02 degree resolution landmask dataset.
11	area of open water i.e. ic 0 (within 50km radius): area radius is calculated using distance (see definition above) and exact pixel size (which is at latitude of 70N about 39km)
12	area of ic 1-10 (within 50km radius)
13	area of ic 10-20 (within 50km radius)
14	area of ic 20-30 (within 50km radius)
15	area of ic 30-40 (within 50km radius)
16	area of ic 40-50 (within 50km radius)
17	area of ic 50-60 (within 50km radius)
18	area of ic 60-70 (within 50km radius)
19	area of ic 70-80 (within 50km radius)
20	area of ic 80-90 (within 50km radius)
21	area of ic 90-100 (within 50km radius)
22	area of ic nan (within 50km radius) nan could mean land or no data (information on the areas on that exact day)
23	time (ordinal, days since 1.1.1, integer value)
24-35	region number 0 ,ice extent and histogram 0 to 100% (like 12-21)
36 -47	region number 1 ,ice extent and histogram 0 to 100% (like 12-21)
48 -59	region number 2 ,ice extent and histogram 0 to 100% (like 12-21)
60 -71	region number 3 ,ice extent and histogram 0 to 100% (like 12-21)
72 -83	region number 4 ,ice extent and histogram 0 to 100% (like 12-21)
84 -95	region number 5 ,ice extent and histogram 0 to 100% (like 12-21)
96-107	region number 6 ,ice extent and histogram 0 to 100% (like 12-21)
108-119	region number 7 ,ice extent and histogram 0 to 100% (like 12-21)
120-131	region number 8 ,ice extent and histogram 0 to 100% (like 12-21)
132-143	region number 9 ,ice extent and histogram 0 to 100% (like 12-21)
144	surface flag of gull position (ocean, land, land water)

After extraction, the above described numpy array is being converted into user-friendly format, e.g. an Excel worksheet. The resolution and characteristics of the extracted data are same as of the initial sea ice dataset. The following figures show some results of the analysis of the extracted dataset.

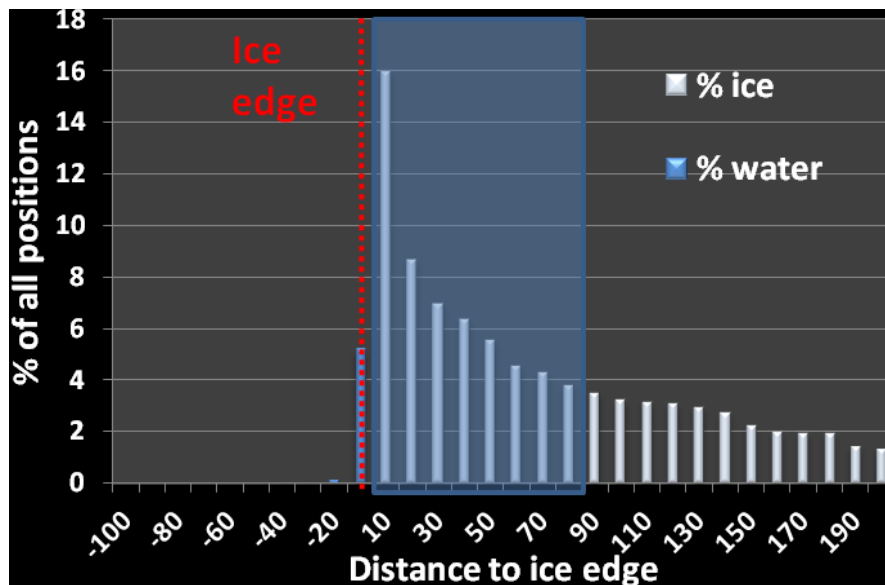


Fig. 9.1: Histogram of the distance to ice edge for the whole set of gull positions.

Fig. 9.1 shows a clear preference of the gulls to stay at the ice edge is visible: less than 6% of all position over open water (and all but a few are within 10km of the ice edge). More than 2/3 of the locations are at less than 100 km from the ice edge.

Fig. 9.2 shows some annual pattern in the behaviour and preference of the gulls. Their preference for lower ice concentrations in spring and higher ice concentrations in summer might be connected to breeding/feeding seasonal behaviour. In case of altered distribution of these ice concentrations in the Arctic Ocean, the seasonal behaviour of the gulls and their locations might be affected. Longer time series of ARGOS positions need to be analysed to track such changes.

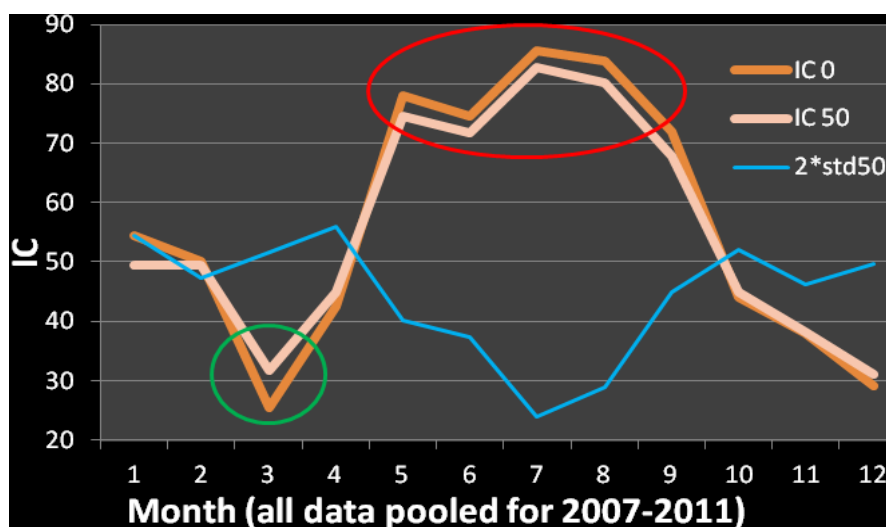


Fig. 9.2: Annual pattern visible: preference for scattered sea ice in March (green circle) and for dense sea ice in summer (red circle), despite limited choice (low SD for IC50 in summer; blue line).

### 9.1.3 Validation methods

As the product consists of the sea ice data extracted for given locations, the validation should address the ASI sea ice concentration algorithm. The algorithm has been developed and validated before the current project activities. The details can be found in the publication by Spreen, G., L. Kaleschke, and G.Heygster (2008), Sea ice remote sensing using AMSR-E 89-GHz channels, *J. Geophys. Res.*, 113, C02S03, doi: 10.1029/2005JC003384.

The consistency of the collocation has been checked via a set of internal consistency tests and does not require any external data source for validation.

**END OF DOCUMENT**